DiVerG: Scalable Distance Index for Validation of Paired-End Alignments in Sequence Graphs

Ali Ghaffaari
Faculty of Technology and Center for Biotechnology (CeBiTec), Bielefeld University, Germany

Alexander Schönhuth
Faculty of Technology and Center for Biotechnology (CeBiTec), Bielefeld University, Germany

Tobias Marschall
Institute for Medical Biometry and Bioinformatics, Medical Faculty, Heinrich Heine University, Düsseldorf, Germany
Center for Digital Medicine, Heinrich Heine University, Düsseldorf, Germany

Abstract

Determining the distance between two loci within a genomic region is a recurrent operation in various tasks in computational genomics. A notable example of this task arises in paired-end read mapping as a form of validation of distances between multiple alignments. While straightforward for a single genome, graph-based reference structures render the operation considerably more involved. Given the sheer number of such queries in a typical read mapping experiment, an efficient algorithm for answering distance queries is crucial. In this paper, we introduce DiVerG, a compact data structure as well as a fast and scalable algorithm, for constructing distance indexes for general sequence graphs on multi-core CPU and many-core GPU architectures. DiVerG is based on PairG [26], but overcomes the limitations of PairG by exploiting the extensive potential for improvements in terms of scalability and space efficiency. As a consequence, DiVerG can process substantially larger datasets, such as whole human genomes, which are unmanageable by PairG. DiVerG offers faster index construction time and consistently faster query time with gains proportional to the size of the underlying compact data structure. We demonstrate that our method performs favorably on multiple real datasets at various scales. DiVerG achieves superior performance over PairG; e.g. resulting to 2.5–4x speed-up in query time, 44–340x smaller index size, and 3–50x faster construction time for the genome graph of the MHC region, as a particularly variable region of the human genome.

The implementation is available at: `https://github.com/cartoonist/diverg`

2012 ACM Subject Classification Mathematics of computing → Paths and connectivity problems; Applied computing → Computational genomics

Keywords and phrases Sequence graph, distance index, read mapping, sparse matrix

Supplementary Material https://github.com/cartoonist/diverg

Funding This project has received funding from the European Union's Horizon 2020 research and innovation programme under the Marie Skłodowska-Curie grant agreement No. 956229.

Acknowledgements This work was supported by the de.NBI Cloud within the German Network for Bioinformatics Infrastructure (de.NBI) and ELIXIR-DE (Forschungszentrum Jülich and W-de.NBI-001, W-de.NBI-004, W-de.NBI-008, W-de.NBI-010, W-de.NBI-013, W-de.NBI-014, W-de.NBI-016, W-de.NBI-022).

1 Introduction

Many genomic studies, such as re-sequencing, have read mapping as their central step in order to place the donor sequence reads into context relative to a reference. Several studies have repeatedly shown that the conventional reference assemblies, i.e. consensus genomes or genomes of individuals, do not capture the genomic diversity of the population and introduce biases [38, 21, 6, 2, 12]. Furthermore, the absence of alternative alleles in a linear reference can penalize correct alignments and lead to decreased accuracy in downstream analysis. To address this issue, augmented reference assembly, often in the form of *pangenome graphs*, have been developed by incorporating genomic variations that is observed in a population [15].

On the other hand, shifting from a linear structure to graph introduces a variety of theoretical challenges. Recent progress in *computational pangenomics* have been paved the way for using such references in practice as established algorithms and data structures for linear references cannot be seamlessly applied to their graphical counterparts [9, 15, 37]. One significant measure affected by this transition is the concept of *distance* between two genomic loci. Defining and computing distance relative to a single genome is inherently straightforward. However, in genome graphs, distance cannot be uniquely defined due to the existence of multiple paths between two loci, with the number of paths being theoretically exponential relative to the number of variants between them.

Determining genomic distances between two loci emerges in several genomic workflows notably paired-end short-read mappings to sequence graphs. In paired-end sequencing, DNA fragments are sequenced from both their ends, where the unsequenced part in between introduces a gap between the sequenced ends. Read mapping is the process of determining where each read originates relative to a reference genome through sequence alignment. There are several sources of ambiguity in finding the correct alignments. The distance between two pairs plays a crucial role in resolving alignment ambiguities, for example in repetitive regions [5]. An accurate alignment of one end can rescue the other end's alignment in case of ambiguities. Therefore, it is important to determine whether the distance between two reference loci, where two ends of a read could be placed, falls in a particular, statistically well motivated range $[d_1, d_2]$. This problem, we refer to as the *Distance Validation Problem (DVP)*, is first formally defined in [26].

The distance between all pairs of candidate alignments corresponding to a paired-end reads should be validated in order to find the correct pairs. Additionally, the candidate alignments in pangenome graphs are often more abundant compared to a linear sequence due to the increased ambiguity in reference genome caused by added variations. This fact, combined with the large number of reads in a typical read mapping workflow, necessitates very efficient methods to answer the DVP, often by preprocessing the graph and constructing an index data structure. Therefore, the efficiency of the involved operation is crucial for rendering short-read-to-graph mapping practically feasible.

Long, third-generation sequencing reads (TGS) have spurred enormous enthusiasm in various domains of application, which may explain that the majority of read-to-graph mapping approaches focuses on such long reads. However, still, long TGS reads are either, if opting for now accurate choices such as PacBio HiFi expensive, or if opting for the cheaper, earlier versions, full of errors; both these issues limit their ranges of applications.

Still, short next-generation sequencing reads are highly accurate, cheap, and available to nearly every sequencing laboratory today. This provides substantial motivation for delivering approaches that render short-read-to-graph mapping a viable option; in fact, this would free the way for usage of graph-based reference systems in many laboratories worldwide. Note, in addition, that despite the great benefits of long reads in resolving sequential ambiguities in repetitive regions, paired-end reads can still provide substantial assistance in this respect.

Related Work

The distance between two nodes in a graph is determined by the paths that connect them and is typically associated with their shortest path. Identifying the shortest paths between two points in a graph is a prevalent problem across various application domains and is one of the extensively studied topics in computer science [14, 17, 18, 23, 25, 39]. However, simply knowing the shortest path length is not always sufficient for addressing the DVP when the length of the shortest path is less than d_1. This is because it cannot determine whether there is a longer path with a length d that satisfies the distance criteria $d_1 \leq d \leq d_2$. On the other hand, the decision version of *longest path problem* and *exact-path length problem*, which respectively answer whether there is a path of at least length d or exactly length d in a graph, are shown to be NP-complete [36, 31].

In the context of sequence graphs, most sequence-to-graph aligners use heuristic approaches to estimate distances [20, 34]. Chang et al. [7] propose an exact method and indexing scheme to determine the minimum distance between any two positions in a sequence graph with a focus on seed clustering. Although their method is shown to be efficient in seed clustering, it cannot address the DVP as it only provides the minimum distance between two positions.

Jain et al. [26] propose PairG, a distance indexing method which, to the best of our knowledge, is the first method directly addressing the DVP. This method, similar to existing approaches, involves preprocessing the graph to create an index that answers distance queries efficiently. In PairG, the index data structure is a sparse Boolean matrix constructed from powers of the adjacency matrix of the graph. Once constructed, it can indicate in near-constant time whether a path exists between two nodes that meet the distance criteria. It benefits from general sparse storage format and employs standard sparse matrix algorithms to reduce space requirement and accelerate the index construction. However, the method cannot scale to handle whole graph genomes for large sequences. PairG, although applicable for small graphs, also fails to run on many-core architectures such as GPU for sparse matrix computations due to its intense memory requirements.

Contributions

In this work, we propose an indexing scheme, referred to as DiVerG, that offers fast exact solutions for the DVP in sequence graphs with significantly lower memory footprint, and faster query and construction time.

DiVerG, enhances PairG in order to overcome the decisive limitations of existing approaches. The first contribution is new *dynamic* compressed formats, namely *rCRS* formats, for storing sparse Boolean matrices. They are *dynamic* in the sense that sparse matrix operations can be conducted directly on matrices in this format without decompression. These formats, although simple by design, provides considerably greater potential for compression of sparse matrices representing the adjacency matrix of sequence graphs, or their powers thereof. The specific incorporation of the logic that supports the shape of adjacency matrices of sequence graphs facilitates significantly more compact representations than what can be achieved by merely utilizing the sparsity of the matrix in standard sparse formats.

Secondly, we propose two algorithms for Boolean sparse matrix multiplication and addition for matrices in rCRS formats, and show that our sparse matrix-matrix multiplication achieves enhanced performance through the bit-level parallelism that the encoded format immediately provides. Moreover, our sparse matrix addition algorithm runs in time proportional to the compressed form.

We also tailored both our algorithms and their corresponding implementations to be particularly powerful on massively parallel architectures, such as GPUs. The faster algorithms and more compacted encodings open up the possibility of indexing matrices reflecting drastically larger graphs, which is infeasible with the prior state of the art. Our experiments show that DiVerG scales favorably with large sequence graphs, at low memory footprint and significant compression ratio. Most importantly, our results demonstrate that DiVerG responds to distance queries in constant time in practice. Despite the prior work, DiVerG's query performance does not grow by the distance constraints parameters.

2 Problem Definition

2.1 Background

Sequence Graphs

Sequence graphs provide compressed representations of sets of similar—evolutionary or environmentally related—genomic sequences [24]. In this work, we consider sequence graphs $G(V, E)$ as node-labelled directed graphs where labels are *single* base pairs and we refer to them as *character graphs*. By definition, in a character graph, the length of a sequence spelt out by a walk of length k is exactly k. Moreover, sequence graphs are defined to be bidirected; i.e. they can be traversed in both forward and reverse directions, which accounts for the complementary structure of genomes. Lastly, a *chain graph* is a character graph that represents a single sequence which is equivalent to the sequential chaining of all (single-letter) nodes. A sequence graph $G(V, E)$ is called *sparse* if the average node degree in G is close to 1.

Paired-end Sequencing

Many next-generation short-read sequencing technologies are capable of generating paired-end reads, which involves sequencing fragments from both ends. Compared to single-end sequencing, paired-end sequencing provides additional information through the distance separating the two ends. Using this information, an accurate alignment of one end can disambiguate the alignment of the other end when multiple alignments are present (Figure 6b in Appendix A). Prior work shows its effectiveness for downstream analyses, particularly in resolving ambiguous alignments in repetitive regions [5]. Fragments in sequencing libraries typically vary in size depending both on the sequencing technology in use and library preparation procedures. In our study, the distance between paired reads in a library is modelled by an interval indicating the expected lower and upper bounds. This interval, which is referred to as *distance constraints*, are assumed to be provided as input parameters. In Appendix A, we discussed how the distance constraints can be determined for a library.

2.2 Distance Validation Problem

Locating the origin of short reads by aligning them to a reference genome, whether linear or graph-based, can be ambiguous due several factors such as repetitive regions in the genome, sequencing errors, and the genetic differences between the donor genome and the reference. In such cases, reads might have multiple candidate alignments. Utilizing the distance information in paired-end sequencing data can help identify the correct alignment.

Two alignments are considered as paired if the probability of the distance between them fit the actual or inferred fragment model. In addition to the distance, the orientation of two paired reads should also be as expected depending on the sequencing technology in use; e.g. one of the pair should be aligned on the forward strand while the other is on the reverse strand.

▶ **Problem 1** (Distance Validation). *Let r_1 and r_2 be two paired reads, and a_1, and a_2 their alignments against a sequence graph $G(V, E)$. Having a_1 mapped to the forward strand implies a_2 to be on the reverse strand. Let v_1 and v_2 be the first nodes in the paths to which a_1 and*

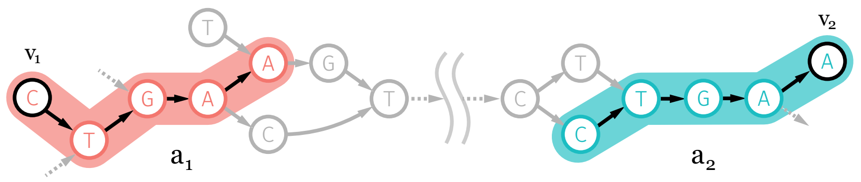

Figure 1 Alignments a_1 and a_2 correspond to a set of paired reads on a sequence graph (partially represented). Alignment a_1 starts from node v_1 and extends along the forward strand, while alignment a_2 starts from v_2 and extends along the reverse complement strand.

a_2 are aligned, respectively (Figure 1). Assuming the fragment model is described by distance constraints (d_1, d_2), the Distance Validation problem is determining whether there exists a path from v_1 to v_2 of length $d \in [d_1, d_2]$. These two alignments are considered as paired *if such condition is met.*

Due to the sheer number of queries in a typical read mapping experiment, the algorithm solving Problem 1 needs to be efficient.

3 k-Walk Matrix as Distance Index

Let $\mathbf{A} = (a_{ij})$ denote the Boolean adjacency matrix of graph $G(V, E)$, defined by $a_{ij} = 1$ if and only if $(i, j) \in E$. The $k-$th power of $\mathbf{A}$ has a special property: $\mathbf{A}^k = (a^k_{uv})$ determines the number of walks of length k between nodes u and v in G. The Boolean equivalent of $\mathbf{A}^k$, which can be achieved by replacing each non-zero entry in $\mathbf{A}^k$ with 1, can answer *existence* queries on walks of length k instead.

For the remainder of the paper, any mentioned adjacency matrices or their k-th powers implicitly refer to Boolean matrices.

▶ **Definition 2** (Boolean Matrix Operations). *Given two Boolean square matrices* $\mathbf{A}$ *and* $\mathbf{B}$ *of order n, standard Boolean matrix operations are defined as follows:*
- *Addition:* $\mathbf{A} \vee \mathbf{B} = a_{i,j} \vee b_{i,j}$*,*
- *Multiplication:* $\mathbf{A} \cdot \mathbf{B} = \bigvee_{k=1}^{n} a_{i,k} \wedge b_{k,j}$*,*
- *Power:* $\mathbf{A}^k = \mathbf{A} \cdot \mathbf{A}^{k-1}$ $(k \neq 0)$*, and* $\mathbf{A}^0 = \mathbf{I}$*,*

where $\vee$ and $\wedge$ are Boolean disjunction (OR) and conjunction (AND) operators.

▶ **Definition 3** (Distance Index). *Given distance constraints (d_1, d_2), a Boolean matrix $\mathcal{T}$ is called* distance index *relative to (d_1, d_2) if defined as:*

$$\mathcal{T} = \mathbf{A}^{d_1} \cdot (\mathbf{A} \vee \mathbf{I})^{d_2 - d_1}, \tag{1}$$

where I is the identity matrix, $\vee$ and $\cdot$ denote Boolean matrix addition and matrix-matrix multiplication, respectively, defined in Definition 2. Jain et al. [26] shows that $\mathcal{T} = (\tau_{ij})$ can efficiently solve the *Distance Validation Problem* defined in Problem 1, i.e. if $\tau_{uv} = 1$, there exists at least one walk of length $d \in [d_1, d_2]$ from node u to v in the graph.

Generally, the diameter of sequence graphs is very large in practice, and the number of edges is on the order of the number of nodes, i.e. $|E| \sim |V|$. This implies that most sequence graphs exhibit sparse adjacency matrices. Therefore, given that distance constraints are considerably smaller than the graph, i.e. $(d_2 - d_1) \ll |V|$, one can expect $\mathcal{T}$ to be sparse. The common approaches for computing Equation (1) leverage the sparsity of the matrices, aiming to operate at time and space complexities proportional to the number of non-zero

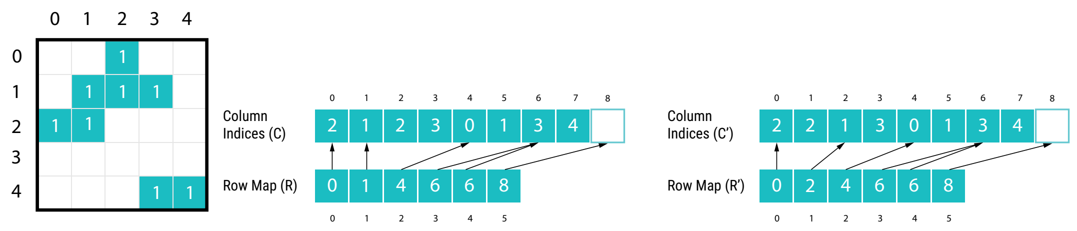

(a) Compressed Row Storage (CRS) **(b)** Range CRS (rCRS)

Figure 2 An example Boolean matrix represented in CRS and rCRS format.

elements. Sparse matrices are typically stored in sparse formats such as the *Compressed Row Storage* (CRS) [4] and the calculation of Equation (1) relies on the sparse matrix-matrix multiplication (SpGEMM) and sparse matrix addition (SpAdd) algorithms [4].

▶ **Definition 4** (Compressed Row Storage). *Given Boolean squared matrix* $\mathbf{A}$ *with* n *rows and* $nnz(\mathbf{A})$ *number of non-zero elements, the* Compressed Row Storage *or* Compressed Sparse Row *format of* $\mathbf{A}$ *is a row-based representation consisting of two one-dimensional arrays* (C, R)*; where*

- C (column indices)*, of size* $nnz(\mathbf{A})$*, stores the column indices of non-zero elements in* $\mathbf{A}$ *in row-wise order;*
- R (row map)*, of length* $n+1$*, maps row index* $i \in [0, n-1]$ *to* $R(i)$ *which is the first position in* C *in which column indices of elements in row* i *are stored. The last value in* R *is set to* $|C|$*, i.e.* $R(n) = nnz(\mathbf{A})$*.*

By definition, array C does not need to be sorted within each partition C_i in CRS format. When the entries of each row in C are sorted, we refer to this as *sorted CRS*. Figure 2a demonstrate a toy example of a Boolean matrix in (sorted) CRS format.

▶ Remark 5. R is defined such that the half-open interval $[R(i), R(i+1))$ indicates the interval in C where all column indices of non-zero elements in row i can be found. Row map R partitions the column indices array C into successive subsequences $C = C_0C_1 \cdots C_{n-1}$, called the *row decomposition* of C. In other words, C_i is subsequence $[C(R(i)) \cdots C(R(i+1)-1)]$ of C which includes column indices of all non-zeros in row i.

The required space for storing sparse matrix $\mathbf{A}_{n\times m}$ in CRS format is $\Theta(n + \mathrm{nnz}(\mathbf{A}))$.

Accessing the element a_{ij} in $\mathbf{A}$ using CRS representation can be reduced to searching for column index j in the part of array C corresponding to row i, as specified by row map array R. That is, one searches for j in C_i, the i-th partition of the row decomposition of C. This search can be facilitated in sorted CRS via binary search, instead of inspecting all column indices in the row. With z being the maximum number of non-zero values in any row in $\mathbf{A}$, searching for j in sorted CRS takes $O(\log(z))$, due to the binary search performed on the sorted entries. As mentioned before, given the sparsity of matrix $\mathbf{A}$, which implies that z is (very) small, accessing elements in sorted-CRS amounts to requiring constant time in practice.

To date, many algorithms have been proposed for parallel sparse matrix-matrix multiplication in formats such as CRS or other similar variants [33, 3]. Since standard matrix operations establish fundamental components of numerous applications, most of them are optimized for various hardware architectures, in particular for architectures that support massive parallelization, such as GPUs. Although the CRS format is often sufficient for general sparse matrix storage and relevant operations, it is computationally prohibitive

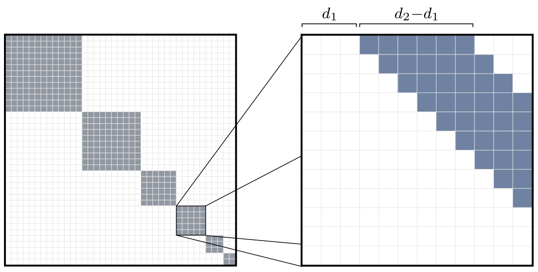

Figure 3 Schematic illustration of the structure of matrix $\mathcal{T}$ with distance constraints $[d_1, d_2]$ for a chain graph with multiple components.

when it is used for computing the k-th power of adjacency matrices as well as the resulting matrix from Equation (1) for large sequence graphs. On the other hand, sequence graph adjacency matrices offer optimization opportunities that are not typically found in general sparse matrices.

3.1 Observations

The distance index $\mathcal{T}$ computed by Equation (1) quickly becomes infeasible for large graphs due to its space requirements. For example, consider a human pangenome graph constructed using the autosomes of the GRCh37 reference genome and incorporating variants from the 1000 Genome Project. Constructing the distance index $\mathcal{T}$ for this graph with distance criteria $d_1 = 150$ and $d_2 = 450$ results in a matrix of order 2.8B with approximately 870B non-zero values. Assuming that each non-zero value consumes 4 bytes, the total space required for the final distance matrix in sorted CRS would be about 3.5 TB.

Even for smaller graphs, storage requirements are impractical for many-core architectures, e.g. GPUs, as they have much smaller memory than the accessible main memory in a CPU. Such many-core architectures are beneficial for faster computation of SpGEMM, which is the computational bottleneck for constructing the distance index.

A key observation for identifying the compression potential is the structure of the distance matrix. Genome graphs usually consist of multiple connected components corresponding to each genomic region or chromosome. If the nodes are indexed such that their indices are *localized* for each region, the distance index $\mathcal{T}$ is a *block-diagonal matrix*, where each block corresponds to a different genomic region or chromosome.

Further examinations reveal that in each row, non-zero values are also localized within a certain range—often grouped into a few clusters of consecutive columns—if nodes are indexed in a “near-topological order”. This is because almost all edges in sequence graphs are local, and it is reflected in the matrix as long as the ordering that defines node indices mostly preserves this locality—i.e. adjacent nodes appear together in the ordering. This observation can be seen clearly in the distance index constructed for a chain graph with distance constraints $[d_1, d_2]$ as shown in Figure 3.

4 Method

4.1 Total Order on Node Set

The nodes of a graph are indexed on the rows of its adjacency matrix with the same order governing columns as well. This inherently defines a total order on the set of nodes in the graph, assigning each node a unique *index*. Different total orders yield different adjacency matrices. Our aim is to find a total order that maximizes the *locality* of the indices in each row. It can be shown that this problem is equivalent to finding a sparse matrix with minimum bandwidth by permuting its rows and columns. In other words, an ordering minimizing the bandwidth of a graph, maximizes the locality of the indices for adjacent nodes. The problem of finding such ordering has been proven to be NP-Complete [32].

As a result, we employ a heuristic approach to find such total order. Assuming the sequence graph is a directed acyclic graph (DAG), we argue that any order induced by the topology of the DAG establishes such an order. Note that, in practice, sequence graphs, particularly variation graphs, are DAGs in the majority of relevant cases. If input sequence graphs are not acyclic, e.g. in de Bruijn graphs, we resort to a "semi-topological ordering" established by "dagifying" the graph, i.e. by running topological sort algorithm on the graph while the traversal algorithm ignores any edges forming a cycle.

Several heuristic algorithms have been proposed to minimize the bandwidth of a sparse matrix by reordering its rows and columns [10, 11, 8] which have not explored in this study. However, in the case of sequence graphs, we expect them to have minimal impact in the final structure of the matrix. Our experimental results (in Section 5) indicate that the ordering achieved by semi-topological sort offers a very effective heuristic. This can be justified by the fact that sequence graphs generally preserve the linear structure of the sequences from which they are constructed, and the variations in these sequences are often only local in the genomic coordinates, thereby affecting the graph locally.

4.2 Range Compressed Row Storage (rCRS)

DiVerG aims to exploit particular properties of the distance index matrix $\mathcal{T}$ mentioned in Section 3.1, as well as its sparsity, to reduce space and time requirements. Our method introduces a new sparse storage format, which will be explained subsequently. This format relies on transforming the standard CRS by replacing column index ranges with their lower and upper bounds to achieve high compression rate. Later, we will propose tailored algorithms to compute sparse matrix operations directly on this compressed data structure without incurring additional overhead for decompression.

▶ **Definition 6** (Minimum Range Sequence). *Let A be a* sorted *sequence of distinct integers. A* "range sequence" *of A is another sequence, A_r, constructed from A in which any disjoint subsequence of consecutive integers is replaced by its first and last values. When such subsequence contains only one integer i, it will be represented as $[i, i]$ in A_r. The minimum sized A_r is defined as* minimum range sequence *of A, denoted as $\rho(A)$.*

▶ **Example 7.** Consider $A = [10, 11, 12, 13, 23, 29, 30]$. It has three disjoint sequence of consecutive integers: 10–13, 23, and 29–30. The minimum range sequence of A is defined as $\rho(A) = [10, 13, 23, 23, 29, 30]$.

▶ **Definition 8** (Range Compressed Row Storage). *For a sparse matrix $\mathbf{A}$ and its sorted CRS representation (C, R), we define Range Compressed Row Storage or rCRS$(\mathbf{A})$ as two 1D arrays (C', R') which are called* column indices *and* row map *arrays respectively:*

- *$C' = \rho(C_0) \cdots \rho(C_{n-1})$, where C_i is partition i in the row decomposition of C;*
- *R' is an array of length $n + 1$, in which $R'(i)$ specifies the start index of $\rho(C_i)$. The last value is defined as $R'(n) = |C'|$.*

It can be easily shown that rCRS can be constructed from sorted CRS in linear time with respect to the number of non-zero values (see Appendix B.1 for more details). Accessing an element in $\mathbf{A}$ represented by rCRS format takes $O(\log(\hat{z}))$ where $\hat{z}$ is the maximum size of each C'_i in row decomposition of C' over all rows i (details in Appendix B.2). Note that, unlike the CRS format, the size of C' is no longer equal to nnz($\mathbf{A}$).

The space complexity of the rCRS representation decisively depends on the distribution of non-zero values in the rows of the matrix (refer to Appendix B.3 for more details). This representation can substantially compress the column indices array C—as low as $O(n)$ compared to $O(nnz(A))$ in CRS—if the array contains long distinct ranges of consecutive integers. The limitation of this representation is that it can be twice as large when there is no stretch of consecutive indices in C. It is important to note that the compression rate can directly influence query time, as it is proportional to the compressed representation of non-zero values.

To mitigate this issue, we define a variant of rCRS, which is referred to as *Asymmetrical Range CRS* (*aCRS*). In the worst case scenario, aCRS format takes as much space as the standard CRS while keeping the same time complexity $O(\log(\hat{z}))$ for the query operation. The aCRS definition and related analysis have been elaborated in Appendix C.

Although aCRS theoretically provides a more compact representation compared to rCRS, the experimental results (in Section 5) shows that it occupies as much space as rCRS when storing distance index $\mathcal{T}$ for sequence graphs in practice. This is due to the fact that the ordering defined in Section 4.1 and the topology of sequence graphs result in isolated column indices being very infrequent. Consequently, aCRS holds two integers per range, similar to rCRS. Considering this fact and the relative ease of implementing efficient sparse matrix algorithms with rCRS in comparison to aCRS, particularly on GPU, we base our implementation on the rCRS format. This can be observed in the index constructed for a chain graph (Figure 3), which often resembles the general structure of sequence graphs.

4.3 Range Sparse Boolean Matrix Multiplication (rSpGEMM)

Given sparse matrices $\mathbf{A}_{m\times n}$ and $\mathbf{B}_{n\times s}$, SpGEMM is an algorithm that computes $\mathbf{C} = \mathbf{A} \cdot \mathbf{B}$ using sparse representations of two input matrices. In this section, we introduce a new SpGEMM algorithm, called *Range SpGEMM* or *rSpGEMM* for short, computing matrix-matrix multiplication when input and output matrices are in the rCRS format. The algorithm is designed to scale well on both multi-core architectures (CPUs) as well as many-core architectures (GPUs).

Similar to most parallel SpGEMM algorithms, our rSpGEMM follows Gustavson's algorithm [22]. Algorithm 1 illustrates its general structure, in which $A(i,:)$ refers to row i of matrix $\mathbf{A}$. This notation can be generalized to $B(j,:)$ and $C(i,:)$ in Algorithm 1 specifying row j and i in B and C, respectively. Note that Algorithm 1 only iterates over non-zeros of $\mathbf{A}$ and $\mathbf{B}$.

The algorithm computes $\mathbf{C}$ one row at a time. To compute $C(i,:)$, it iterates over non-zero values in row $A(i,:)$ and computes its contribution to $C(i,:)$ by multiplying it to non-zero values in row B_j; i.e. the term $a_{ij} \cdot B(j,:)$ in Line 3. This contribution is then *accumulated* with the partial results computed from previous iterations. The row accumulation can be simplified to $C(i,:) \leftarrow C(i,:) + B(j,:)$ in Boolean matrices as a_{ij} is 1.

Since computing each row of the final matrix is independent of the others, $\mathbf{C} = \mathbf{A} \cdot \mathbf{B}$ can be seen as multiple independent vector-matrix multiplication $C(i,:) = A(i,:) \cdot \mathbf{B}$. For simplicity, we will only focus on the equivalent vector-matrix multiplication.

Given that the output matrix is also in the sparse format, knowing the number of non-zero values in each row of $\mathbf{C}$ is essential before storing the calculated C_i in the final matrix. This issue is usually tackled using a two-phase approach: firstly, the *symbolic* phase, delineates the

Algorithm 1 Gustavson's algorithm.

```
Require: Sparse matrices $\mathbf{A}_{n\times m}$ and $\mathbf{B}_{m\times s}$
1: for $i \in [0, m)$ do
2:     for $a_{ij} \in A(i,:)$ do
3:         $C(i,:) \leftarrow C(i,:) + a_{ij} \cdot B(j,:)$
```

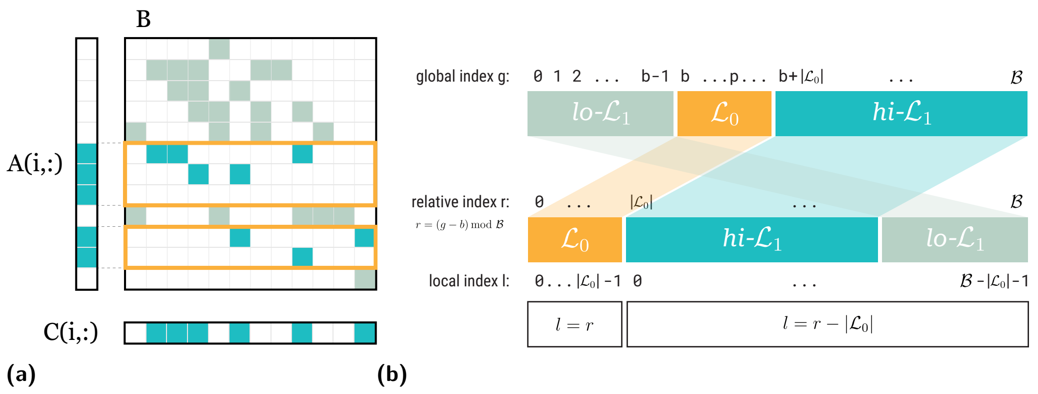
B
A(i,:)
C(i,:)
(a)
(b)
global index g:
0 1 2 ... b-1 b ...p... b+|$\mathcal{L}_0$| ... $\mathcal{B}$
lo-$\mathcal{L}_1$
$\mathcal{L}_0$
hi-$\mathcal{L}_1$
relative index r:
$r = (g - b) \bmod \mathcal{B}$
0 ... |$\mathcal{L}_0$| ... $\mathcal{B}$
$\mathcal{L}_0$
hi-$\mathcal{L}_1$
lo-$\mathcal{L}_1$
local index l:
0...|$\mathcal{L}_0$|-1 0 ... $\mathcal{B}$-|$\mathcal{L}_0$|-1
$l = r$
$l = r - |\mathcal{L}_0|$

Figure 4 (a) Row accumulation in Boolean matrices can be viewed as the union of all non-zero values in rows of **B** that are specified by the non-zero values in A_i. (b) BBB hierarchical structure and indexing.

structure of **C**, primarily corresponding to the computation of its row map array. Secondly, the *numeric* phase, carries out the actual computation of **C**.

Similar to SpGEMM algorithms based on Gustavson's, the fundamental aspect of rSpGEMM resides in three anchor points: the data structure employed for row accumulation, memory access pattern to minimize data transfer latency, and distribution of work among threads in hierarchical parallelism. In the following, we address each of these points.

4.3.1 Bi-Level Banded Bitvector as Accumulator

The row accumulation in Boolean SpGEMM, explained in Section 4.3, can be seen as the union of all column indices in $B(j,:)$ for all j where $a_{ij} \neq 0$. Figure 4a schematically depicts the row accumulation in computing a row of the final matrix. It is important to highlight that row accumulation in rSpGEMM is carried out on ranges of indices that are, by definition, disjoint and sorted (Remark 24).

Our method employs a dense bitvector, namely *Bi-level Banded Bitvector* (BBB), as an accumulator in rSpGEMM. From a high-level point of view, this bitvector supports two main operations: `scatter` and `gather`. The `scatter` operation stores a range of column indices at once, which essentially involves setting a range of sequential bits in the bitvector to one. Conversely, the `gather` operation retrieves the union of column indices stored by the `scatter` method in the form of the minimum range sequence (Definition 6). Computing $C(i,:)$ is essentially a combination of `scatter`ing partial results and `gather`ing the final accumulated entries using BBB.

The `scatter` operation is a bit-parallel operation that sets bits corresponding to index range $[s, f]$ in a series of W-bit operations. Each set bit in the bitvector indicates absence/presence of the corresponding column in the final result. The pseudocode of the `scatter` can be found in Algorithm 5.

Each cluster of set bits in the final bitvector represents an interval in the final row $C(i,:)$, with each interval corresponding to an entry pair in the rCRS format. In the symbolic phase, the `gather` operation counts the number of entries in rCRS with regards to non-zeros in row $C(i,:)$. In the numeric phase, it constructs the resulting row as a minimum range sequence. In order to avoid scanning all words for set bits, the absolute minimum ($j_{\min}$) and maximum ($j_{\max}$) word indices are tracked and the final scan is limited to $[j_{\min}, j_{\max}]$. Since each row in $\mathbf{B}$ is sorted, $j_{\min}$ and $j_{\max}$ are updated once per row. Algorithm 6 demonstrates the pseudocodes of the `gather` operations in the symbolic and numeric phrase. The `gather` operation also exploits bit parallelism and operates using four trivial bitwise functions: `cnt`, `map01`, `map10`, and `sel`.

The `cnt` function simply counts the number of set bits in a word and is performed by a single machine instruction (`POPCNT`). The `map01` function marks the first bit of any consecutive set bits in a word to one by keeping all `01` occurrences in a word and mapping all other combinations (i.e. `00`, `10`, and `11`) to `00`. The `map10` function marks the bit immediately after the last bit of any consecutive set bits in a word to one by mapping all `10` occurrences to `01` in a word and other combinations to `00`. Both `map01` and `map10` can be calculated using basic bitwise operations in constant time independent of the word size. The `sel`(x, i) function gives the position of i-th set bit in word x relying on native machine instructions (e.g. `__fns` intrinsic in CUDA and `PDEP` and `TZCNT` instructions on CPUs). Additional information regarding these operations can be found in Appendix D.1.

The bitvector is designed to perform well in scenarios where non-zeros in row $C(i,:)$ are localized, which reflects a practically common scenario. To this end, two design decisions have been made. Firstly, the size of the bitvector is bounded by the bandwidth observed in $C(i,:)$ which is calculated before the symbolic phase. Secondly, the bitvector is partitioned into two levels $\mathcal{L}_0$ and $\mathcal{L}_1$ in order to minimize the memory latency by utilizing the locality of non-zero values in $C(i,:)$. The first level ($\mathcal{L}_0$) is allocated on the fast (low-latency) memory if there is hardware support (e.g. shared memory in GPUs). The rest of the bit fields is mapped to the second level $\mathcal{L}_1$ and allocated on the larger memory but with higher latency (e.g. global memory on GPU). On hardware where software-managed memory hierarchy is not available (like CPUs), this model promotes cache-friendly memory accesses.

The rationale behind this design is that the first level $\mathcal{L}_0$ spans the range of bits that are more likely to be accessed during row accumulations. If all non-zero values in a row are bound to $\mathcal{L}_0$ index range, no words in $\mathcal{L}_1$ are fetched or modified. Therefore, all `scatter` and `gather` operations mentioned earlier are performed on words in the fastest memory. The relative position of the first level within a row is specified by the index of its center bit p, referred as *pivot bit.* For example, the center of the band in each row of C is a viable option for p. In this work, we chose $p = i$ to set the $\mathcal{L}_0$ region around the diagonal as node i is more likely to be adjacent to nodes with ranks close to i in adjacency matrices.

The arrangement of bits in two levels necessitates calculating internal (local) indices within levels from column (global) indices. Local indices in each level are calculated from corresponding global indices relative to p and using module arithmetic (see Figure 4b and Appendix D.2 for more details).

4.3.2 Partitioning Schemes

Consider computing $\mathbf{C} = \mathbf{A} \cdot \mathbf{B}$ using rSpGEMM with matrices in rCRS format, there are different ways to distribute required work units among available threads. The partitioning and assignment of work units to computational units can influence the runtime, memory usage, and memory access patterns. Additionally, our implementation benefits from the

Kokkos library [13] to achieve performance portability, meaning that it can be executed on multiple supported hardware architectures. As different hardware can impose different requirements, an efficient partitioning strategy on a specific architecture is not necessarily efficient on another.

Inspired by [13], we examined different strategies: *Thread-Sequential, Team-Sequential*, and *Thread-Parallel* partitioning schemes, which are described in detail in Appendix E.

4.4 Range Sparse Boolean Matrix Addition (rSpAdd)

In this section, we shift our focus to calculating matrix-matrix addition in rCRS format which is required for computing the distance index. We propose *Range Boolean Sparse Add* (or *rSpAdd*) algorithm which computes matrix $\mathbf{C} = \mathbf{A} \vee \mathbf{B}$ where all matrices are in rCRS format and $\vee$ is Boolean matrix addition defined in Definition 2.

Considering that non-zero values in each row of rCRS matrices are represented by ranges, each with two integers (Remark 12), and these integers are sorted and disjoint (Remark 13), row $C(i,:)$ is equivalent to the sorted combination of ranges in both rows $A(i,:)$ and $B(i,:)$, where overlapping ranges are collapsed into one. For each row in $\mathbf{C}$, this is achieved by using two pointers, each initially pointing to the first element of the respective rows. The algorithm peeks at the pairs in $A(i,:)$ and $B(i,:)$ indicated by the pointers. If two ranges are disjoint, it inserts the one with smaller bounds in $C(i,:)$ and increments the pointer indicating the inserted pair by two. If two ranges overlap, they will be merged by inserting the minimum of lower bounds and the maximum of upper bounds of the two pointed elements into $C(i,:)$ in that order. Then, both pointers are incremented to indicate the next pairs. In case either pointer reaches the end of the row, the remaining elements from the other row are directly appended to $C(i,:)$.

The time complexity of this algorithm is bound by compressed representation of input matrices in rCRS format. Since the ranges in rCRS are disjoint and sorted, merging two rows $A(i,:)$ and $B(i,:)$ can be done in $\Theta(|A(i,:)| + |B(i,:)|)$; in which $|A(i,:)|$ and $|B(i,:)|$ are the sizes of $A(i,:)$ and $B(i,:)$ in rCRS format, respectively. rSpAdd not only requires smaller working space compared to SpAdd but is arguably faster due to compressed representation of the matrices.

4.5 Distance Index

As stated in Section 3.1, the distance index constructed by Equation (1) is a block-diagonal matrix. For this reason, DiVerG builds the distance index incrementally for each block; i.e. computing the distance matrix for each component of the sequence graph individually. The adjacency matrix for each component can be constructed in rCRS format one row at a time. Therefore, it is not required to store the whole matrix in sorted CRS format to be able to convert it to rCRS. Once matrices $\mathbf{A}$ and $\mathbf{I}$ are in rCRS format, $\mathcal{T}$ can be computed using rSpAdd and rSpGEMM. The powers of $\mathbf{A}$ and $\mathbf{A} \vee \mathbf{I}$ are computed using “exponentiation by squaring” [27]. Ultimately, matrix $\mathcal{T}$ is further compressed by encoding both the column indices and row map arrays using Elias-δ encoding [16].

5 Experimental Results

5.1 Implementation

DiVerG is implemented in C++17. The matrix $\mathcal{T}$, in the final stage, is converted to *encoded rCRS* format (described in Section 4.5) whose size is reported as *index size* in Section 5.3. Our implementation relies on Kokkos [13] for performance portability across different architectures, and we specifically focused on two execution spaces: OpenMP (for CPU), and CUDA (for GPU).

We compared the performance of our algorithm with PairG which uses `kkSpGEMM` meta-algorithm implemented in Kokkos [13] for computing sparse matrix multiplication. Kokkos offers several algorithms for computing SpGEMM. `kkSpGEMM` algorithm attempts to choose the best algorithm one based on the inputs. The implementation of PairG, although technically possible, but required some modification in higher-levels for running on GPU. Our comparisons with PairG in this section relies on this reimplementation.

All CPU experiments were conducted on an instance on de.NBI cloud with a 28-core (one thread per core) Intel® Xeon® Processor running Ubuntu 22.4. Distance index construction on GPU were carried out on another instance with an NVIDIA A40 GPU running Ubuntu 22.4. In Appendix F, we report the results of tuning the meta-parameters of DiVerG.

5.2 Datasets

DiVerG is assessed using seven different graphs. Four of these graphs were previously employed by PairG in their evaluation, while three additional graphs have been introduced to address significantly larger and more complex scenarios. Together, these graphs span over a spectrum of scales, complexities, and construction methods.

Three of these graphs are variation graphs of different regions of the human genome, constructed from small variants in the 1000 Genomes Project [1] based on GRCh37 reference assembly: mitochondrial DNA (mtDNA) graph, BRCA1 gene graph (BRC), and the killer cell immunoglobulin-like receptors (LRC_KIR) graph. One graph is a de Bruijn graph constructed using whole-genome sequences of 20 strains of B. *anthracis*. We added three new variation graphs to this ensemble: MHC region graph constructed from alternate loci released with GRCh38 reference assembly [35], and HPRC CHM13 graph [29] constructed by minigraph. More details about these datasets are reported in Appendix G; particularly, Table 3 presents some statistics of the sequence graphs used in our evaluation.

5.3 Results

We evaluate the *index size* (`size`), *construction time* (`ctime`), and high water mark memory footprint during index construction (`mem`) for different distance constraints using the graphs explained in Section 5.2. In addition, the *query time* is measured for the distance index by averaging the time spend for querying 1M randomly sampled paired positions throughout each graph. Our method is evaluated using two separate sets of distance constraints.

Performance Evaluation with Increasing Distance Constraints Intervals

In the first experiment, performance metrics are computed for two graphs, BRCA1 (small) and MHC (medium-sized), with distance constraints: [0–128], [0–256], [0–512], and [0–1024]. This experiment reveals the behaviour of our algorithm as the distance range increases and specifically highlights the performance of *rSpGEMM* in computing the term $(\mathbf{A} \vee \mathbf{I})^{d_2-d_1}$ in Equation (1), which is a bottleneck in calculating $\mathcal{T}$. The performance measures are computed on both CPU (OpenMP) and GPU (CUDA).

Figure 5a illustrates the performance measures and their comparison with PairG for the BRCA1 graph. As can be seen, DiVerG is about 4–7x faster in query time and 45–172x smaller in size in comparison to standard sparse matrix format and operations. Furthermore, the results show that DiVerG is approximately 9–28x faster than PairG in construction time

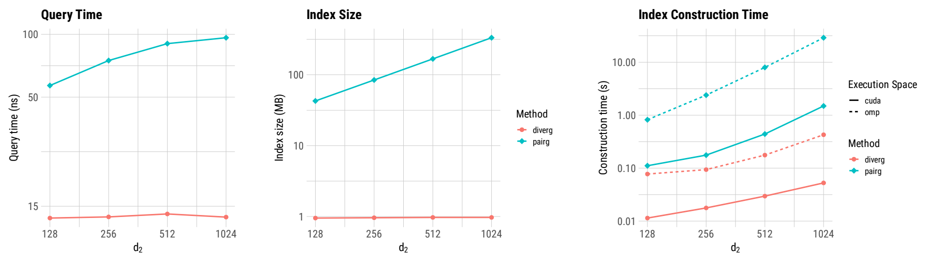

(a)

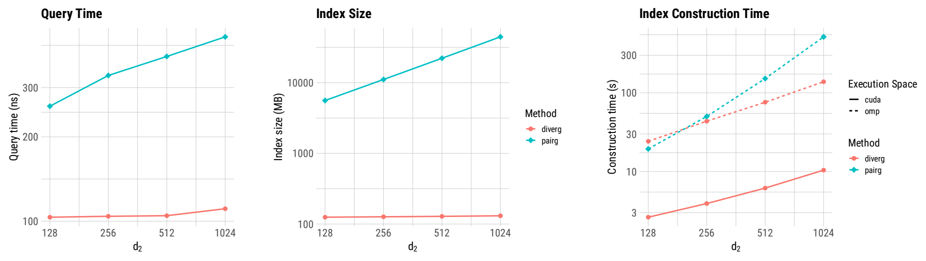

(b)

Figure 5 Log-scale Performance of DiVerG for BRCA1 (a) and MHC graphs (b).

on GPU and 10–68x on CPU. Moreover, the query time and index size in DiVerG do not change as the range of the distance constraints increases. This is because the number of non-zero values, i.e. ranges, in the rCRS format saturates quickly and stays constant.

Our evaluations for MHC region graph conducted with the same distance intervals are illustrated in Figure 5b. Although MHC being is much larger than the BRCA1 graph, the trends in the results remain consistent. Specifically, DiVerG achieves about 2.5–4x speed-up in accessing matrix; the index in the rCRS format is approximately 44–340x smaller compared to the classical CRS format; and the query time and index size do not change with an increase in the distance interval. As the standard SpGEMM in PairG fails to construct the index on GPU due to the large size of the graph and the limited memory available on the device, we only report the runtime on CPU for this graph.

As shown in Figure 5b, DiVerG is faster that PairG in indexing the graph on CPU, except for the distance interval [0, 128]. However, as the distance intervals grow larger, DiVerG becomes up to 3x faster in index construction. This speedup increases to 7–49.5x when DiVerG is executed on GPU: 7x for the distance constraint [0, 128] and 49.5x for [0, 1024].

Performance Evaluation with Offset Distance Constraints Intervals

In the second experiments, DiVerG is assessed for more realistic distance constraints [0–250], [150–450], and [350–650], resembling the inner distance model for paired-end reads with fragment sizes 300 bp, 500 bp, and 700 bp, respectively. In order to demonstrate the scalability of DiVerG for large whole genome, we indexed chr1 and chr22 of the HPRC CHM13 graph. All benchmarks are executed on a NVIDIA A40 GPU which has a 48 GB of global memory. For certain datasets and parameter configurations, PairG failed to construct the index, either due to excessive memory requirements or because it did not complete within a 6-hour time frame. In those cases, we only report the performance of DiVerG for this graph in Table 1 and the size of PairG index is computed via direct conversion from rCRS to CRS.

Table 1 Performance of DiVerG compared to PairG on an NVIDIA A40 GPU in terms of index size (`size`), construction time (`ctime`), high water mark memory footprint (`mem`), and query time (`qtime`), along with the number of non-zero values in the final index (`nnz`).

			DiVerG				PairG			
	d_1–d_2	`nnz`	`size`	`ctime`	`mem`	`qtime`	`size`	`ctime`	`mem`	`qtime`
mtDNA	0–250	7M	**287**KB	**37**ms	**1**MB	**12**ns	52MB	215ms	2.17GB	36ns
	150–450	8M	**245**KB	**39**ms	**1**MB	**11**ns	60MB	240ms	2.18GB	37ns
	350–650	8M	**243**KB	**39**ms	**1**MB	**11**ns	58MB	239ms	2.18GB	36ns
BRCA1	0–250	21M	**1**MB	**35**ms	**4**MB	**13**ns	164MB	113ms	542MB	69ns
	150–450	26M	**1**MB	**41**ms	**5**MB	**13**ns	197MB	173ms	500MB	75ns
	350–650	26M	**1**MB	**44**ms	**5**MB	**13**ns	197MB	176ms	500MB	75ns
LRC	0–250	290M	**13**MB	**320**ms	**52**MB	**25**ns	2.2GB	1.1s	4.5GB	113ns
	150–450	349M	**13**MB	**374**ms	**70**MB	**25**ns	2.7GB	1.9s	5.4GB	120ns
	350–650	350M	**13**MB	**394**ms	**73**MB	**22**ns	2.7GB	1.9s	5.5GB	117ns
MHC	0–250	3B	**125**MB	**8**s	**41**GB	**53**ns	21GB	11s	44GB	164ns
	150–450	3B	**126**MB	**11**s	**41**GB	**57**ns	26GB	–	–	–
	350–650	3B	**127**MB	**13**s	**41**GB	**55**ns	26GB	–	–	–
B.Anth.	0–250	5B	**178**MB	**4**m**22**s	**43**GB	**59**ns	34GB	–	–	–
	150–450	9B	**221**MB	**11**m**18**s	**43**GB	**59**ns	66GB	–	–	–
	350–650	14B	**254**MB	**23**m**49**s	**43**GB	**60**ns	104GB	–	–	–
chr22	0–250	16B	**723**MB	**37**s	**34**GB	**60**ns	121GB	–	–	–
	150–450	20B	**737**MB	**52**s	**33**GB	**57**ns	149GB	–	–	–
	350–650	21B	**743**MB	**58**s	**34**GB	**57**ns	154GB	–	–	–
chr1	0–250	66B	**2.96**GB	**14**m**18**s	**43**GB	**63**ns	495GB	–	–	–
	150–450	80B	**3**GB	**45**m**35**s	**43**GB	**62**ns	601GB	–	–	–
	350–650	82B	**3**GB	**1**h**04**m	**43**GB	**62**ns	612GB	–	–	–

Table 1 shows the superior performance of DiVerG in all metrics, being about 170–420x smaller, and, in instances where PairG successfully completes, the indices are created 3–6x faster with considerably lower memory requirements than PairG for all datasets. The average number of column indices in each row in the rCRS format is about 2.1 for all variation graphs and all distance intervals. This number is approximately 4.8, 5.8, and 8.2 for the de Bruijn graph with distance intervals [0–250], [150–450], and [350, 650], respectively, while the average number of non-zero values per row in the equivalent CRS format is close to 300, i.e. $d_2 - d_1$. This explains the high compression ratio of the DiVerG distance index. Additionally, the query time has seen a 3–5x speedup across all pangenome graphs. Our method can handle significantly larger graphs that are beyond the capabilities of PairG as it only requires a few tens of megabytes *auxiliary space* in memory per active thread.

6 Conclusion

In this work, we have proposed DiVerG, a compressed representation combined with fast algorithms for computing a distance index that leverages significant potential for space and runtime efficiency observed in adjacency matrices of sequence graphs. DiVerG provided a fast solution for the prominent DVP in paired-end read mapping to pangenome graphs. Our extensive experiments showed that DiVerG facilitates the computation of distance indexes, making it possible to solve the DVP when working with large graphs. We have demonstrated how to optimize algorithms with respect to hardware architecture considerations, which has been crucial for processing graphs that capture genomes at the scale of various eukaryotic genomes. We developed DiVerG with a particular focus on aligning paired-end short-reads to graphs, recognizing that the DVP can be a computational bottleneck. In the future, we plan to employ DiVerG in the context of sequence-to-graph alignments.

References

1 A. Auton, G. R. Abecasis, D. M. Altshuler, R. M. Durbin, D. R. Bentley, A. Chakravarti, A. G. Clark, P. Donnelly, E. E. Eichler, P. Flicek, S. B. Gabriel, R. A. Gibbs, E. D. Green, M. E. Hurles, B. M. Knoppers, J. O. Korbel, E. S. Lander, C. Lee, H. Lehrach, E. R. Mardis, G. T. Marth, G. A. McVean, D. A. Nickerson, J. P. Schmidt, S. T. Sherry, J. Wang, R. K. Wilson, E. Boerwinkle, H. Doddapaneni, Y. Han, V. Korchina, C. Kovar, S. Lee, D. Muzny, J. G. Reid, Y. Zhu, Y. Chang, Q. Feng, X. Fang, X. Guo, M. Jian, H. Jiang, X. Jin, T. Lan, G. Li, J. Li, Y. Li, S. Liu, X. Liu, Y. Lu, X. Ma, M. Tang, B. Wang, G. Wang, H. Wu, R. Wu, X. Xu, Y. Yin, D. Zhang, W. Zhang, J. Zhao, M. Zhao, X. Zheng, N. Gupta, N. Gharani, L. H. Toji, N. P. Gerry, A. M. Resch, J. Barker, L. Clarke, L. Gil, S. E. Hunt, G. Kelman, E. Kulesha, R. Leinonen, W. M. McLaren, R. Radhakrishnan, A. Roa, D. Smirnov, R. E. Smith, I. Streeter, A. Thormann, I. Toneva, B. Vaughan, X. Zheng-Bradley, R. Grocock, S. Humphray, T. James, Z. Kingsbury, R. Sudbrak, M. W. Albrecht, V. S. Amstislavskiy, T. A. Borodina, M. Lienhard, F. Mertes, M. Sultan, B. Timmermann, M. L. Yaspo, L. Fulton, R. Fulton, V. Ananiev, Z. Belaia, D. Beloslyudtsev, N. Bouk, C. Chen, D. Church, R. Cohen, C. Cook, J. Garner, T. Hefferon, M. Kimelman, C. Liu, J. Lopez, P. Meric, C. O'Sullivan, Y. Ostapchuk, L. Phan, S. Ponomarov, V. Schneider, E. Shekhtman, K. Sirotkin, D. Slotta, H. Zhang, S. Balasubramaniam, J. Burton, P. Danecek, T. M. Keane, A. Kolb-Kokocinski, S. McCarthy, J. Stalker, M. Quail, C. J. Davies, J. Gollub, T. Webster, B. Wong, Y. Zhan, C. L. Campbell, Y. Kong, A. Marcketta, F. Yu, L. Antunes, M. Bainbridge, A. Sabo, Z. Huang, L. J. Coin, L. Fang, Q. Li, Z. Li, H. Lin, B. Liu, R. Luo, H. Shao, Y. Xie, C. Ye, C. Yu, F. Zhang, H. Zheng, H. Zhu, C. Alkan, E. Dal, F. Kahveci, E. P. Garrison, D. Kural, W. P. Lee, W. F. Leong, M. Stromberg, A. N. Ward, J. Wu, M. Zhang, M. J. Daly, M. A. DePristo, R. E. Handsaker, E. Banks, G. Bhatia, Angel G. Del, G. Genovese, H. Li, S. Kashin, S. A. McCarroll, J. C. Nemesh, R. E. Poplin, S. C. Yoon, J. Lihm, V. Makarov, S. Gottipati, A. Keinan, J. L. Rodriguez-Flores, T. Rausch, M. H. Fritz, A. M. Stütz, K. Beal, A. Datta, J. Herrero, G. R. Ritchie, D. Zerbino, P. C. Sabeti, I. Shlyakhter, S. F. Schaffner, J. Vitti, D. N. Cooper, E. V. Ball, P. D. Stenson, B. Barnes, M. Bauer, R. K. Cheetham, A. Cox, M. Eberle, S. Kahn, L. Murray, J. Peden, R. Shaw, E. E. Kenny, M. A. Batzer, M. K. Konkel, J. A. Walker, D. G. MacArthur, M. Lek, R. Herwig, L. Ding, D. C. Koboldt, D. Larson, K. Ye, S. Gravel, A. Swaroop, E. Chew, T. Lappalainen, Y. Erlich, M. Gymrek, T. F. Willems, J. T. Simpson, M. D. Shriver, J. A. Rosenfeld, C. D. Bustamante, S. B. Montgomery, La Vega F. M. De, J. K. Byrnes, A. W. Carroll, M. K. DeGorter, P. Lacroute, B. K. Maples, A. R. Martin, A. Moreno-Estrada, S. S. Shringarpure, F. Zakharia, E. Halperin, Y. Baran, E. Cerveira, J. Hwang, A. Malhotra, D. Plewczynski, K. Radew, M. Romanovitch, C. Zhang, F. C. Hyland, D. W. Craig, A. Christoforides, N. Homer, T. Izatt, A. A. Kurdoglu, S. A. Sinari, K. Squire, C. Xiao, J. Sebat, D. Antaki, M. Gujral, A. Noor, E. G. Burchard, R. D. Hernandez, C. R. Gignoux, D. Haussler, S. J. Katzman, W. J. Kent, B. Howie, A. Ruiz-Linares, E. T. Dermitzakis, S. E. Devine, H. M. Kang, J. M. Kidd, T. Blackwell, S. Caron, W. Chen, S. Emery, L. Fritsche, C. Fuchsberger, G. Jun, B. Li, R. Lyons, C. Scheller, C. Sidore, S. Song, E. Sliwerska, D. Taliun, A. Tan, R. Welch, M. K. Wing, X. Zhan, P. Awadalla, A. Hodgkinson, X. Shi, A. Quitadamo, G. Lunter, J. L. Marchini, S. Myers, C. Churchhouse, O. Delaneau, A. Gupta-

Hinch, W. Kretzschmar, Z. Iqbal, I. Mathieson, A. Menelaou, A. Rimmer, D. K. Xifara, T. K. Oleksyk, Y. Fu, M. Xiong, L. Jorde, D. Witherspoon, J. Xing, B. L. Browning, S. R. Browning, F. Hormozdiari, P. H. Sudmant, E. Khurana, C. Tyler-Smith, C. A. Albers, Q. Ayub, Y. Chen, V. Colonna, L. Jostins, K. Walter, Y. Xue, M. B. Gerstein, A. Abyzov, S. Balasubramanian, J. Chen, D. Clarke, A. O. Harmanci, M. Jin, D. Lee, J. Liu, X. J. Mu, J. Zhang, Y. Zhang, C. Hartl, K. Shakir, J. Degenhardt, S. Meiers, B. Raeder, F. P. Casale, O. Stegle, E. W. Lameijer, I. Hall, V. Bafna, J. Michaelson, E. J. Gardner, R. E. Mills, G. Dayama, K. Chen, X. Fan, Z. Chong, T. Chen, M. J. Chaisson, J. Huddleston, M. Malig, B. J. Nelson, N. F. Parrish, B. Blackburne, S. J. Lindsay, Z. Ning, H. Lam, C. Sisu, D. Challis, U. S. Evani, J. Lu, U. Nagaswamy, J. Yu, W. Li, Kang H. Min, L. Habegger, H. Yu, F. Cunningham, I. Dunham, K. Lage, J. B. Jespersen, H. Horn, D. Kim, R. Desalle, A. Narechania, M. A. Sayres, F. L. Mendez, G. D. Poznik, P. A. Underhill, L. Coin, D. Mittelman, R. Banerjee, M. Cerezo, T. W. Fitzgerald, S. Louzada, A. Massaia, F. Yang, D. Kalra, W. Hale, X. Dan, K. C. Barnes, C. Beiswanger, H. Cai, H. Cao, B. Henn, D. Jones, J. S. Kaye, A. Kent, A. Kerasidou, R. Mathias, P. N. Ossorio, M. Parker, C. N. Rotimi, C. D. Royal, K. Sandoval, Y. Su, Z. Tian, S. Tishkoff, M. Via, Y. Wang, H. Yang, L. Yang, J. Zhu, W. Bodmer, G. Bedoya, Z. Cai, Y. Gao, J. Chu, L. Peltonen, A. Garcia-Montero, A. Orfao, J. Dutil, J. C. Martinez-Cruzado, R. A. Mathias, A. Hennis, H. Watson, C. McKenzie, F. Qadri, R. LaRocque, X. Deng, D. Asogun, O. Folarin, C. Happi, O. Omoniwa, M. Stremlau, R. Tariyal, M. Jallow, F. S. Joof, T. Corrah, K. Rockett, D. Kwiatkowski, J. Kooner, T. T. Hiên, S. J. Dunstan, N. T. Hang, R. Fonnie, R. Garry, L. Kanneh, L. Moses, J. Schieffelin, D. S. Grant, C. Gallo, G. Poletti, D. Saleheen, A. Rasheed, L. D. Brooks, A. L. Felsenfeld, J. E. McEwen, Y. Vaydylevich, A. Duncanson, M. Dunn, and J. A. Schloss. A global reference for human genetic variation. *Nature*, 526(7571):68–74, oct 2015. URL: `https://www.ncbi.nlm.nih.gov/pubmed/26432245`, `doi:10.1038/nature15393`.

2 Débora Y. C. Brandt, Vitor R. C. Aguiar, Bárbara D. Bitarello, Kelly Nunes, Jérôme Goudet, and Diogo Meyer. Mapping Bias Overestimates Reference Allele Frequencies at the HLA Genes in the 1000 Genomes Project Phase I Data. *G3: Genes, Genomes, Genetics*, 5(5):931–941, mar 2015. URL: `https://www.ncbi.nlm.nih.gov/pubmed/25787242`, `doi:10.1534/g3.114.015784`.

3 Aydin Buluç and John R. Gilbert. Parallel Sparse Matrix-Matrix Multiplication and Indexing: Implementation and Experiments. *SIAM Journal on Scientific Computing*, 34(4):C170–C191, January 2012. URL: `https://epubs.siam.org/doi/abs/10.1137/110848244?casa_token=WVToSvZW2ssAAAAA:IDgyMJqVg3bxHWJVTQLnqJOp-6mfhovxRe_9dasAnqLl8A-hM8jjdRcam9A8iWPNyHniT25Xtic`, `doi:10.1137/110848244`.

4 Aydın Buluç, John Gilbert, and Viral B. Shah. *Implementing Sparse Matrices for Graph Algorithms*, pages 287–313. Society for Industrial and Applied Mathematics (SIAM), 2011. URL: `https://epubs.siam.org/doi/abs/10.1137/1.9780898719918.ch13`, `arXiv:https://epubs.siam.org/doi/pdf/10.1137/1.9780898719918.ch13`, `doi:10.1137/1.9780898719918.ch13`.

5 Stefan Canzar and Steven L. Salzberg. Short Read Mapping: An Algorithmic Tour. *Proceedings of the IEEE*, 105(3):436–458, mar 2017. `doi:10.1109/jproc.2015.2455551`.

6 Mark J. P. Chaisson, Ashley D. Sanders, Xuefang Zhao, Ankit Malhotra, David Porubsky, Tobias Rausch, Eugene J. Gardner, Oscar L. Rodriguez, Li Guo, Ryan L. Collins, Xian Fan, Jia Wen, Robert E. Handsaker, Susan Fairley, Zev N. Kronenberg, Xiangmeng Kong, Fereydoun Hormozdiari, Dillon Lee, Aaron M. Wenger, Alex R. Hastie, Danny Antaki, Thomas Anantharaman, Peter A. Audano, Harrison Brand, Stuart Cantsilieris, Han Cao, Eliza Cerveira, Chong Chen, Xintong Chen, Chen-Shan Chin, Zechen Chong, Nelson T. Chuang, Christine C. Lambert, Deanna M. Church, Laura Clarke, Andrew Farrell, Joey Flores, Timur Galeev, David U. Gorkin, Madhusudan Gujral, Victor Guryev, William Haynes Heaton, Jonas Korlach, Sushant Kumar, Jee Young Kwon, Ernest T. Lam, Jong Eun Lee, Joyce Lee, Wan-Ping Lee, Sau Peng Lee, Shantao Li, Patrick Marks, Karine Viaud-Martinez, Sascha Meiers,

Katherine M. Munson, Fabio C. P. Navarro, Bradley J. Nelson, Conor Nodzak, Amina Noor, Sofia Kyriazopoulou-Panagiotopoulou, Andy W. C. Pang, Yunjiang Qiu, Gabriel Rosanio, Mallory Ryan, Adrian Stütz, Diana C. J. Spierings, Alistair Ward, AnneMarie E. Welch, Ming Xiao, Wei Xu, Chengsheng Zhang, Qihui Zhu, Xiangqun Zheng-Bradley, Ernesto Lowy, Sergei Yakneen, Steven McCarroll, Goo Jun, Li Ding, Chong Lek Koh, Bing Ren, Paul Flicek, Ken Chen, Mark B. Gerstein, Pui-Yan Kwok, Peter M. Lansdorp, Gabor T. Marth, Jonathan Sebat, Xinghua Shi, Ali Bashir, Kai Ye, Scott E. Devine, Michael E. Talkowski, Ryan E. Mills, Tobias Marschall, Jan O. Korbel, Evan E. Eichler, and Charles Lee. Multi-platform discovery of haplotype-resolved structural variation in human genomes. *Nature Communications*, 10(1), April 2019. URL: https://www.nature.com/articles/s41467-018-08148-z, doi:10.1038/s41467-018-08148-z.

7 Xian Chang, Jordan Eizenga, Adam M. Novak, Jouni Sirén, and Benedict Paten. Distance Indexing and Seed Clustering in Sequence Graphs. *Bioinformatics*, 36(Supplement 1):i146–i153, July 2020. arXiv:https://academic.oup.com/bioinformatics/article-pdf/36/Supplement_1/i146/33488679/btaa446.pdf, doi:10.1093/bioinformatics/btaa446.

8 K. Y. Cheng. Minimizing the bandwidth of sparse symmetric matrices. *Computing*, 11(2):103–110, 1973. URL: https://link.springer.com/article/10.1007/BF02252900, doi:10.1007/BF02252900.

9 Computational Pan-Genomics Consortium. Computational pan-genomics: status, promises and challenges. *Briefings in Bioinformatics*, 19(1):118–135, January 2018. URL: https://academic.oup.com/bib/article/19/1/118/2566735, doi:10.1093/bib/bbw089.

10 E. Cuthill and J. McKee. Reducing the bandwidth of sparse symmetric matrices. In *Proceedings of the 1969 24th National Conference*, ACM '69, page 157–172, New York, NY, USA, 1969. Association for Computing Machinery. URL: https://dl.acm.org/doi/10.1145/800195.805928, doi:10.1145/800195.805928.

11 Elizabeth Cuthill. *Several Strategies for Reducing the Bandwidth of Matrices*, pages 157–166. Springer US, Boston, MA, 1972. URL: https://link.springer.com/chapter/10.1007/978-1-4615-8675-3_14, doi:10.1007/978-1-4615-8675-3_14.

12 Jacob F. Degner, John C. Marioni, Athma A. Pai, Joseph K. Pickrell, Everlyne Nkadori, Yoav Gilad, and Jonathan K. Pritchard. Effect of read-mapping biases on detecting allele-specific expression from RNA-sequencing data. *Bioinformatics*, 25(24):3207–3212, October 2009. URL: https://academic.oup.com/bioinformatics/article/25/24/3207/235151, doi:10.1093/bioinformatics/btp579.

13 Mehmet Deveci, Christian Trott, and Sivasankaran Rajamanickam. Multi-threaded Sparse Matrix-Matrix Multiplication for Many-Core and GPU Architectures, 2018. URL: https://arxiv.org/abs/1801.03065, doi:10.48550/ARXIV.1801.03065.

14 E. W. Dijkstra. A note on two problems in connexion with graphs. *Numerische Mathematik*, 1(1):269–271, December 1959. URL: https://link.springer.com/article/10.1007/BF01386390, doi:10.1007/bf01386390.

15 Jordan M. Eizenga, Adam M. Novak, Jonas A. Sibbesen, Simon Heumos, Ali Ghaffaari, Glenn Hickey, Xian Chang, Josiah D. Seaman, Robin Rounthwaite, Jana Ebler, Mikko Rautiainen, Shilpa Garg, Benedict Paten, Tobias Marschall, Jouni Sirén, and Erik Garrison. Pangenome Graphs. *Annual Review of Genomics and Human Genetics*, 21(1), may 2020. doi:10.1146/annurev-genom-120219-080406.

16 P. Elias. Universal codeword sets and representations of the integers. *IEEE Transactions on Information Theory*, 21(2):194–203, March 1975. URL: https://ieeexplore.ieee.org/document/1055349, doi:10.1109/tit.1975.1055349.

17 Michael L. Fredman and Robert Endre Tarjan. Fibonacci heaps and their uses in improved network optimization algorithms. *Journal of the ACM*, 34(3):596–615, July 1987. URL: https://dl.acm.org/doi/10.1145/28869.28874, doi:10.1145/28869.28874.

18 Giorgio Gallo and Stefano Pallottino. Shortest path algorithms. *Annals of Operations Research*, 13(1):1–79, December 1988. URL: https://link.springer.com/article/10.1007/BF02288320, doi:10.1007/bf02288320.

19 Erik Garrison and Andrea Guarracino. Unbiased pangenome graphs. *bioRxiv*, feb 2022. URL: https://www.biorxiv.org/content/10.1101/2022.02.14.480413v1, doi:10.1101/2022.02.14.480413.

20 Erik Garrison, Jouni Sirén, Adam M. Novak, Glenn Hickey, Jordan M. Eizenga, Eric T. Dawson, William Jones, Shilpa Garg, Charles Markello, Michael F. Lin, Benedict Paten, and Richard Durbin. Variation graph toolkit improves read mapping by representing genetic variation in the reference. *Nature Biotechnology*, 36(9):875–879, aug 2018. doi:10.1038/nbt.4227.

21 Cristian Groza, Tony Kwan, Nicole Soranzo, Tomi Pastinen, and Guillaume Bourque. Personalized and graph genomes reveal missing signal in epigenomic data. *Genome Biology*, 21(1):124, May 2020. URL: https://genomebiology.biomedcentral.com/articles/10.1186/s13059-020-02038-8, doi:10.1186/s13059-020-02038-8.

22 Fred G. Gustavson. Two Fast Algorithms for Sparse Matrices: Multiplication and Permuted Transposition. *ACM Transactions on Mathematical Software*, 4(3):250–269, sep 1978. URL: https://dl.acm.org/doi/10.1145/355791.355796, doi:10.1145/355791.355796.

23 Peter Hart, Nils Nilsson, and Bertram Raphael. A Formal Basis for the Heuristic Determination of Minimum Cost Paths. *IEEE Transactions on Systems Science and Cybernetics*, 4(2):100–107, July 1968. URL: https://ieeexplore.ieee.org/document/4082128, doi:10.1109/tssc.1968.300136.

24 J. Hein. A new method that simultaneously aligns and reconstructs ancestral sequences for any number of homologous sequences, when the phylogeny is given. *Molecular Biology and Evolution*, 6(6):649–668, 11 1989. arXiv:https://academic.oup.com/mbe/article-pdf/6/6/649/11167687/6hein.pdf, doi:10.1093/oxfordjournals.molbev.a040577.

25 Moritz Hilger, Ekkehard Köhler, Rolf Möhring, and Heiko Schilling. Fast Point-to-Point Shortest Path Computations with Arc-Flags. In Camil Demetrescu, Andrew V. Goldberg, and David S. Johnson, editors, *The Shortest Path Problem, Proceedings of a DIMACS Workshop, Piscataway, New Jersey, USA, November 13-14, 2006*, volume 74 of *DIMACS Series in Discrete Mathematics and Theoretical Computer Science*, pages 41–72. DIMACS/AMS, July 2006. doi:10.1090/dimacs/074/03.

26 Chirag Jain, Haowen Zhang, Alexander Dilthey, and Srinivas Aluru. Validating Paired-End Read Alignments in Sequence Graphs. In Katharina T. Huber and Dan Gusfield, editors, *19th International Workshop on Algorithms in Bioinformatics (WABI 2019)*, volume 143 of *Leibniz International Proceedings in Informatics (LIPIcs)*, pages 17:1–17:13, Dagstuhl, Germany, 2019. Schloss Dagstuhl–Leibniz-Zentrum fuer Informatik. URL: http://drops.dagstuhl.de/opus/volltexte/2019/11047, doi:10.4230/LIPIcs.WABI.2019.17.

27 Donald E. Knuth. *The Art of Computer Programming: Seminumerical Algorithms*, volume 2, chapter 4. Addison-Wesley Longman Publishing Co., Inc., USA, third edition, 1997.

28 Heng Li, Xiaowen Feng, and Chong Chu. The design and construction of reference pangenome graphs with minigraph. *Genome Biology*, 21(1):265, oct 2020. doi:10.1186/s13059-020-02168-z.

29 Wen-Wei Liao, Mobin Asri, Jana Ebler, Daniel Doerr, Marina Haukness, Glenn Hickey, Shuangjia Lu, Julian K. Lucas, Jean Monlong, Haley J. Abel, Silvia Buonaiuto, Xian H. Chang, Haoyu Cheng, Justin Chu, Vincenza Colonna, Jordan M. Eizenga, Xiaowen Feng, Christian Fischer, Robert S. Fulton, Shilpa Garg, Cristian Groza, Andrea Guarracino, William T. Harvey, Simon Heumos, Kerstin Howe, Miten Jain, Tsung-Yu Lu, Charles Markello, Fergal J. Martin, Matthew W. Mitchell, Katherine M. Munson, Moses Njagi Mwaniki, Adam M. Novak, Hugh E. Olsen, Trevor Pesout, David Porubsky, Pjotr Prins, Jonas A. Sibbesen, Jouni Sirén, Chad Tomlinson, Flavia Villani, Mitchell R. Vollger, Lucinda L. Antonacci-Fulton, Gunjan Baid, Carl A. Baker, Anastasiya Belyaeva, Konstantinos Billis, Andrew Carroll, Pi-Chuan Chang, Sarah Cody, Daniel E. Cook, Robert M. Cook-Deegan, Omar E. Cornejo, Mark Diekhans, Peter

Ebert, Susan Fairley, Olivier Fedrigo, Adam L. Felsenfeld, Giulio Formenti, Adam Frankish, Yan Gao, Nanibaa' A. Garrison, Carlos Garcia Giron, Richard E. Green, Leanne Haggerty, Kendra Hoekzema, Thibaut Hourlier, Hanlee P. Ji, Eimear E. Kenny, Barbara A. Koenig, Alexey Kolesnikov, Jan O. Korbel, Jennifer Kordosky, Sergey Koren, HoJoon Lee, Alexandra P. Lewis, Hugo Magalhães, Santiago Marco-Sola, Pierre Marijon, Ann McCartney, Jennifer McDaniel, Jacquelyn Mountcastle, Maria Nattestad, Sergey Nurk, Nathan D. Olson, Alice B. Popejoy, Daniela Puiu, Mikko Rautiainen, Allison A. Regier, Arang Rhie, Samuel Sacco, Ashley D. Sanders, Valerie A. Schneider, Baergen I. Schultz, Kishwar Shafin, Michael W. Smith, Heidi J. Sofia, Ahmad N. Abou Tayoun, Françoise Thibaud-Nissen, Francesca Floriana Tricomi, Justin Wagner, Brian Walenz, Jonathan M. D. Wood, Aleksey V. Zimin, Guillaume Bourque, Mark J. P. Chaisson, Paul Flicek, Adam M. Phillippy, Justin M. Zook, Evan E. Eichler, David Haussler, Ting Wang, Erich D. Jarvis, Karen H. Miga, Erik Garrison, Tobias Marschall, Ira M. Hall, Heng Li, and Benedict Paten. A draft human pangenome reference. *Nature*, 617(7960):312–324, May 2023. URL: `https://www.nature.com/articles/s41586-023-05896-x#citeas`, `arXiv:https://www.biorxiv.org/content/10.1101/2022.07.09.499321v1`, `doi:10.1038/s41586-023-05896-x`.

30 Shoshana Marcus, Hayan Lee, and Michael C. Schatz. SplitMEM: a graphical algorithm for pan-genome analysis with suffix skips. *Bioinformatics*, 30(24):3476–3483, December 2014. URL: `http://bioinformatics.oxfordjournals.org/content/30/24/3476`, `doi:10.1093/bioinformatics/btu756`.

31 Matti Nykänen and Esko Ukkonen. The Exact Path Length Problem. *Journal of Algorithms*, 42(1):41–53, jan 2002. `doi:10.1006/jagm.2001.1201`.

32 Ch. H. Papadimitriou. The NP-Completeness of the bandwidth minimization problem. *Computing*, 16(3):263–270, September 1976. URL: `https://link.springer.com/article/10.1007/BF02280884`, `doi:10.1007/bf02280884`.

33 Md. Mostofa Ali Patwary, Nadathur Rajagopalan Satish, Narayanan Sundaram, Jongsoo Park, Michael J. Anderson, Satya Gautam Vadlamudi, Dipankar Das, Sergey G. Pudov, Vadim O. Pirogov, and Pradeep Dubey. Parallel Efficient Sparse Matrix-Matrix Multiplication on Multicore Platforms. In Julian M. Kunkel and Thomas Ludwig, editors, *High Performance Computing*, volume 9137, pages 48–57, Cham, 2015. Springer International Publishing. URL: `https://link.springer.com/chapter/10.1007/978-3-319-20119-1_4`, `doi:10.1007/978-3-319-20119-1_4`.

34 Mikko Rautiainen and Tobias Marschall. GraphAligner: rapid and versatile sequence-to-graph alignment. *Genome Biology*, 21(1):253, September 2020. URL: `https://genomebiology.biomedcentral.com/articles/10.1186/s13059-020-02157-2`, `doi:10.1186/s13059-020-02157-2`.

35 Valerie A. Schneider, Tina Graves-Lindsay, Kerstin Howe, Nathan Bouk, Hsiu-Chuan Chen, Paul A. Kitts, Terence D. Murphy, Kim D. Pruitt, Françoise Thibaud-Nissen, Derek Albracht, Robert S. Fulton, Milinn Kremitzki, Vincent Magrini, Chris Markovic, Sean McGrath, Karyn Meltz Steinberg, Kate Auger, William Chow, Joanna Collins, Glenn Harden, Timothy Hubbard, Sarah Pelan, Jared T. Simpson, Glen Threadgold, James Torrance, Jonathan M. Wood, Laura Clarke, Sergey Koren, Matthew Boitano, Paul Peluso, Heng Li, Chen-Shan Chin, Adam M. Phillippy, Richard Durbin, Richard K. Wilson, Paul Flicek, Evan E. Eichler, and Deanna M. Church. Evaluation of GRCh38 and de novo haploid genome assemblies demonstrates the enduring quality of the reference assembly. *Genome Research*, 27(5):849–864, April 2017. URL: `https://genome.cshlp.org/content/27/5/849.full`, `doi:10.1101/gr.213611.116`.

36 Alexander Schrijver. *Combinatorial optimization.* Number 24 in Algorithms and combinatorics. Springer, Berlin, 2003.

37 Ting Wang, Lucinda Antonacci-Fulton, Kerstin Howe, Heather A. Lawson, Julian K. Lucas, Adam M. Phillippy, Alice B. Popejoy, Mobin Asri, Caryn Carson, Mark J. P. Chaisson, Xian Chang, Robert Cook-Deegan, Adam L. Felsenfeld, Robert S. Fulton, Erik P. Garrison, Nanibaa' A. Garrison, Tina A. Graves-Lindsay, Hanlee Ji, Eimear E. Kenny, Barbara A. Koenig, Daofeng Li, Tobias Marschall, Joshua F. McMichael, Adam M. Novak, Deepak Purushotham, Valerie A. Schneider, Baergen I. Schultz, Michael W. Smith, Heidi J. Sofia, Tsachy Weissman, Paul Flicek, Heng Li, Karen H. Miga, Benedict Paten, Erich D. Jarvis, Ira M. Hall, Evan E. Eichler, and David Haussler. The Human Pangenome Project: a global resource to map genomic diversity. *Nature*, 604(7906):437–446, April 2022. URL: `https://www.nature.com/articles/s41586-022-04601-8#citeas`, `doi:10.1038/s41586-022-04601-8`.

38 Xuefang Zhao, Ryan L. Collins, Wan-Ping Lee, Alexandra M. Weber, Yukyung Jun, Qihui Zhu, Ben Weisburd, Yongqing Huang, Peter A. Audano, Harold Wang, Mark Walker, Chelsea Lowther, Jack Fu, Mark B. Gerstein, Scott E. Devine, Tobias Marschall, Jan O. Korbel, Evan E. Eichler, Mark J. P. Chaisson, Charles Lee, Ryan E. Mills, Harrison Brand, and Michael E. Talkowski. Expectations and blind spots for structural variation detection from long-read assemblies and short-read genome sequencing technologies. *The American Journal of Human Genetics*, 108(5):919–928, May 2021. URL: `https://www.cell.com/ajhg/fulltext/S0002-9297(21)00098-7`, `doi:10.1016/j.ajhg.2021.03.014`.

39 Uri Zwick. Exact and Approximate Distances in Graphs — A Survey. In Friedhelm Meyer auf der Heide, editor, *Algorithms — ESA 2001*, pages 33–48, Berlin, Heidelberg, 2001. Springer Berlin Heidelberg. `doi:10.1007/3-540-44676-1_3`.

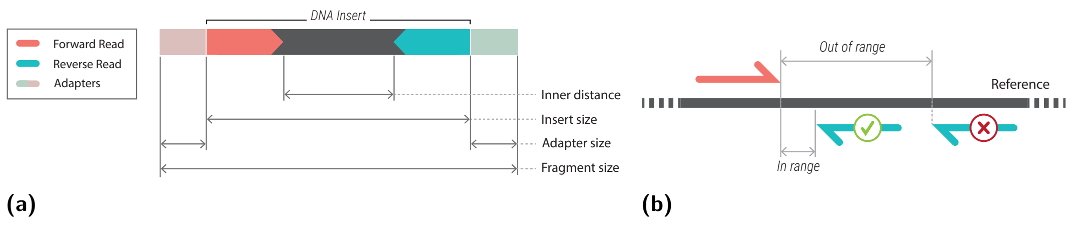

Figure 6 (a) A fragment in paired-end sequencing: a DNA insert with two adapters attached at each end enabling sequencing from both ends. (b) A schematic example of resolving alignment ambiguities using distance validation. The forward read has an unique alignment (in red) which can determine the correct alignment of the other end (blue).

A Fragment Model in Paired-End Sequencing

In paired-end sequencing, read libraries are created by attaching sequencing adapters at both ends of DNA segments (inserts), enabling sequencing from both ends. This results in producing two reads per fragment. One read, referred to as *forward read*, extends along the forward strand of the DNA insert. The other one, termed *reverse read* extends from the other end on the reverse complementary strand (Figure 6a).

The fragment model of a read library describes the probability distribution of the insert sizes. This model is typically denoted by a normal distribution, characterized by the empirical mean and variance of the insert sizes.

In our study, the fragment model is represented by the lower and upper bounds of the expected insert size instead of a probability distribution. These bounds are still probabilistic, as they refer to reasonably chosen cut-offs on the tails of the insert size distribution, e.g. capturing 99.7% of the observed lengths or defined as $\mu \pm 3\sigma$ in which μ and σ are mean and variance in the fragment model.

There are two ways to define the distance between two paired reads. The *inner distance* between the ends of two paired reads which is determined by the size of unsequenced part of the DNA fragment. It can be calculated by subtracting the sum of the read lengths from the insert size (as shown in Figure 6a). The *outer distance* is defined by the distance between the starts of two paired reads which is equivalent to the *insert size*. Given the variability in both insert sizes and read lengths, and the possibility of overlapping reads in some datasets, using the outer distance simplifies the process of distance validation. Therefore, validating outer distance is more practical compared to the inner distance. Nevertheless, the method is neutral with respect to either definition of distance.

B Range Compressed Row Storage (rCRS) Analysis

B.1 rCRS Construction

▶ **Lemma 9.** *The minimum range sequence of a non-empty set of integers A can be constructed from the sorted array representing A in linear time.*

Proof. It can be trivially constructed by starting from $\rho(A) = \emptyset$ and iterating over elements in A in ascending order. In iteration i, if $a_i \neq a_{i-1} + 1$ or $i = 1$, a_i will be added to $\rho(A)$. The constructed $\rho(A)$ is minimum in size since it can be easily shown that any other set with smaller cardinality implies the membership of some elements not actually in A (by contradiction). ◀

▶ **Lemma 10.** *Given A as a non-empty set of integers, the size of the minimum range sequence of A is at least 2 and at most twice the cardinality of A; specifically, $2 \leq |\rho(A)| \leq 2|A|$.*

Proof. This follows directly from the fact that any range sequence of A defines a partition of A, denoted as P, where each block in P represents a contiguous range of integers in A. For each block in P, $\rho(A)$ contains exactly two integers. Thus, $2 \leq |\rho(A)| = 2|P| \leq 2|A|$ holds because the number of blocks $|P|$ is at least 1 and at most $|A|$. ◀

▶ **Theorem 11.** *rCRS can be constructed from sorted CRS in linear time with respect to the number of non-zero values.*

Proof. It directly follows Definition 8 and Lemma 9 (see Algorithm 2). ◀

Algorithm 2 Construction of rCRS matrix from CRS one.

```
Require: Sparse matrix $\mathbf{A}_{n\times m}$ in CRS format
 1: function CrsToRCrs($\mathbf{A}$)
 2:     $C' \leftarrow []$
 3:     $R' \leftarrow [0]$
 4:     for $i \leftarrow 0$ to $n$ do
 5:         $b \leftarrow \mathbf{A}.R[i]$
 6:         $e \leftarrow \mathbf{A}.R[i+1]$
 7:         while $b \neq e$ do
 8:             $s \leftarrow \mathbf{A}.C[b]$
 9:             while $\mathbf{A}.C[b] = \mathbf{A}.C[b]+1$ do
10:                 $b \leftarrow b+1$
11:             $C'$.append($s$)
12:             $C'$append($\mathbf{A}.C[b]$)
13:             $b \leftarrow b+1$
14:         $R'$.append($|C'|$)
15:     $A' \leftarrow (C', R')$
16:     report $A'$
```

B.2 Query Time Analysis

▶ Remark 12. In the column indices array C' of rCRS, each element can be identified as either a lower or an upper bound of a range based on its index. Specifically, odd indices refer to lower bounds, whereas even indices refer to upper bounds.

▶ Remark 13. The elements of the column indices array in rCRS, C', are sorted and the ranges indicated by pairs in it are disjoint.

▶ **Theorem 14.** *Let $\hat{z}$ be the maximum size of the minimum range sequence representation over rows of sparse matrix $\mathbf{A}$. Accessing an element in $\mathbf{A}$ represented by rCRS format takes $O(\log(\hat{z}))$.*

Proof. Similar to CRS, accessing element a_{ij} in matrix $\mathbf{A}$ is equivalent to searching j in C'_i—partition i in row decomposition of C'. By definition, the size of C'_i is even and each two elements at indices $2k-1$ and $2k$ in C' for any $k \in \mathbb{N}$ forms a *range* of column indices; i.e. they represent a cluster of non-zero values in row i which occur at columns $C'[2k-1]\ldots C'[2k]$ (Remark 12). The pseudocode for the algorithm is given in Algorithm 3. The loop (at Line 5) finds the index of the last range in C'_i whose lower bound is smaller than or equal to j using binary search. This index, stored as p in the pseudocode (Line 6), represents the lower bound of the identified range; meaning $C'[p] \leq j$. Based on Remark 13, it can be easily shown that all pairs other than $[C'[p], C'[p+1]]$ do not contain j. Therefore, the range specified by p can determine the presence of j in C'. The algorithm clearly takes $O(\log(\hat{z}))$ time in the worst case scenario, where $\hat{z}$ is the maximum size of C'_i over all rows i. ◀

Algorithm 3 Querying rCRS matrix.

```
Require: Sparse matrix $\mathbf{M}$ in rCRS format, row index $i$, and column index $j$
 1: function QueryRCrs($\mathbf{M}$, $i$, $j$)
 2:     $b \leftarrow \mathbf{M}.R'[i]$
 3:     $e \leftarrow \mathbf{M}.R'[i+1]$
 4:     $l \leftarrow e - b$
 5:     while $l > 2$ do
 6:         $p \leftarrow b + l/2$
 7:         if $\mathbf{M}.C'[p] \leq j$ then
 8:             $b \leftarrow p$
 9:         $l \leftarrow l/2$
10:     report $(p \neq e)$ and $\mathbf{M}.C'[p] \leq j \leq \mathbf{M}.C'[p+1]$
```

B.3 Storage Space Analysis

The space complexity of the rCRS representation decisively depends on the distribution of non-zero values in the rows of the matrix. Since the row map arrays of both rCRS and CRS formats are the same size, only the column indices array C' is the effective factor in compression rate of rCRS compared to the standard CRS.

▶ **Theorem 15.** *For a sparse matrix $A_{n\times m}$, the column indices array C' in the rCRS representation requires storage space that is at least $2n$ and at most twice the storage needed by the standard CRS format.*

Proof. Directly followed by Lemma 10 for each row of A. ◀

C Asymmetrical Range CRS

Asymmetrical Range CRS (aCRS) is defined similar to the CRS format with slight tweaks to avoid redundancy in the column indices array when there is an isolated column index x, which is otherwise stored as subsequence $[x, x]$ in rCRS.

▶ **Definition 16** (Minimum Asymmetrical Range Sequence). *Let A be a* sorted *sequence of distinct positive integers, and A_s a sequence constructed by replacing any disjoint subsequence of consecutive integers $S = s_f \cdots s_l$ in A by s_f and $-s_l$ if $|S| > 1$; otherwise S is replaced by the single element s_f. The sequence of minimum size constructed this way is defined as the* minimum asymmetrical range sequence *of A and is denoted by $\hat{\rho}(A)$.*

▶ **Example 17.** Let $A = [10, 11, 12, 13, 23, 29, 30]$ from previous example. The minimum asymmetrical range sequence of A is defined as $\hat{\rho}(A) = [10, -13, 23, 29, -30]$.

▶ **Lemma 18.** *The minimum asymmetrical range sequence of a non-empty set of integers A can be constructed from the sorted array representing A in linear time.*

Proof. It can be trivially shown similar to Lemma 9. ◀

▶ **Lemma 19.** *Given A as a non-empty set of positive integers, the size of the minimum asymmetrical range sequence of A is at most equal to the cardinality of A; i.e. $|\hat{\rho}(A)| \leq |A|$.*

Proof. Similar to Lemma 10, $\hat{\rho}(A)$ defines a partition of A, as each element $a \in A$ belongs to a unique range in $\hat{\rho}(A)$. Therefore, its size is upper bounded by $|A|$. ◀

▶ **Definition 20** (Asymmetrical Range Compressed Row Storage). *For a sparse matrix $\mathbf{A}$ and its sorted CRS representation (C, R), Asymmetrical Range Compressed Row Storage or aCRS$(\mathbf{A})$ is defined as two arrays (C'', R''); where*

- *$C'' = \hat{\rho}(C_0)\hat{\rho}(C_1)\cdots\hat{\rho}(C_{n-1})$, in which C_i is the ith partition in row decomposition of C;*
- *R'' is an array of length $n+1$ in which $R'(i)$ specifies the start index in C'' that corresponds to row i; i.e. the start index of $\hat{\rho}(C_i)$. The last value is defined as $R''(n) = |C'|$.*

▶ Remark 21. Since column indices are non-negative, negative values in aCRS distinctly indicate the upper bound of a range.

▶ **Theorem 22.** *aCRS can be constructed from sorted CRS in linear time with respect to the number of non-zero values.*

Proof. Directly followed by Lemma 18 and Definition 20. ◀

▶ **Theorem 23.** *For a sparse matrix $\mathbf{A}$, aCRS$(\mathbf{A})$ always requires space that is equal to or smaller than that of CRS($\mathbf{A}$) as well as rCRS($\mathbf{A}$).*

Proof. This can be readily demonstrated using Lemma 19 and Definition 20. ◀

▶ Remark 24. The elements of the column indices array in aCRS, C'', are sorted in each partition of its row decomposition and the ranges indicated by pairs or isolated elements in C''_i are disjoint.

▶ **Theorem 25.** *Let $\hat{z}$ be the maximum size of the minimum asymmetrical range sequence representation over rows of sparse matrix $\mathbf{A}$. Accessing an element in $\mathbf{A}$ represented by aCRS format takes $O(\log(\hat{z}))$.*

Proof. Querying element $a_{i,j}$ of $\mathbf{A}$ stored in aCRS format can be done in a similar way as rCRS by searching j in the subsequence of C'' corresponding to row i; i.e. C''_i. The pseudocode for querying aCRS matrices are given in Algorithm 4. We, first, find the last element in C''_i that is smaller than or equal to j using binary search. This element is either an upper bound or a lower bound of a range of non-zero values which can be identified by its sign (Remark 21). It is important to note that we compare j with the *absolute value* of the elements in C'' (Algorithm 4). Assume p is such an index which should belong to a range in the form of $[C''[p], C''[p+1]]$ or $[C''[p]]$. Based on Remark 24, it can be shown that other ranges other than p found by the binary search do not contain j. Therefore, the range specified by p can determine the presence of j in C''; that is if $j \leq C''[p]$, then $a_{i,j} = 1$; otherwise the answer is zero. ◀

Algorithm 4 Querying aCRS matrix.

```
Require: Sparse matrix $\mathbf{M}$ in aCRS format, row index $i$, and column index $j$
function QueryACrs($\mathbf{M}$, $i$, $j$)
    $b \leftarrow \mathbf{M}.R'[i]$
    $e \leftarrow \mathbf{M}.R'[i+1]$
    $l \leftarrow e - b$
    while $l > 0$ do
        $m \leftarrow l/2$
        $p \leftarrow b + m$
        if abs($\mathbf{M}.C'[p]$) $< j$ then
            $b \leftarrow p + 1$
            $l \leftarrow l - m - 1$
        else
            $l \leftarrow m$
    if $M.C'[p] < 0$ then
        $p \leftarrow p - 1$
    report $(p \neq e)$ and $\mathbf{M}.C'[p] <= j$
```

D Bi-Level Banded Bitvector

D.1 `scatter` and `gather` Operations

In this section, we cover some details regarding the `scatter` and `gather` operations (Algorithm 5 and Algorithm 6).

As we stated before, the `gather` operation exploits bit parallelism and relies on using four bitwise functions: `cnt`, `map01`, `map10`, and `sel`. The `map*` functions can be computed using basic bitwise operations [1] as demonstrated in Algorithm 6. The border cases, when `01` or `10` occur at the boundaries between two words, are handled by peeking at the immediate bit on the left of the bit that is being processed. In other words, the most significant bit (MSB) of the previous word is appended to the current word before applying `map*` functions. This bit, which is called *carried* bit, is zero for the first word.

In the symbolic phase, `gather` counts the number of entries in rCRS with regards to non-zeros in row $C(i,:)$. This count is equivalent to twice the number of `01` occurrences in the bitvector and can be formulated as `cnt`(`map01`(w)) for all modified words w in the bitvector. In order to convert the set bit stretches to integer intervals in numeric phase, the first and the last bit of each stretch are marked by applying `map01` and `map10` functions on all words. Finally, calling `sel` on each set bits in (`map01`(w) OR `map10`(w)) gets the final minimum range sequence of the accumulated indices.

As explained, applying `sel` on bits marked by `map10` gives the index immediately after the last set bit in a set bit sequence. These values should be subtracted by one as the integer intervals in rCRS are closed meaning that the upper bounds are inclusive. Since the upper bounds are always written on odd indices of column indices array, bits corresponding to upper bounds can be detected and adjusted based on their indices in the array.

▶ **Example 26.** Consider the 16-bit word $w = \texttt{00}\underline{\texttt{1111}}\texttt{00}\underline{\texttt{11}}\texttt{00}\underline{\texttt{111}}\texttt{0}$ representing the bitvector resulted from `scatter` operations, which essentially denotes the absence/presence of column

[1] `http://www-graphics.stanford.edu/~seander/bithacks.html`

indices in the final row. Then, we have $\texttt{map01}(w) = \texttt{0010000010001000}$, in which all bits except the occurrences of $\texttt{01}$ are set to 0 and $\texttt{map10}(w) = \texttt{0000001000100001}$, in which all occurrences of $\texttt{10}$ are retained as $\texttt{01}$ and the rest of bits are set to zero. It can be seen that the number of intervals with consecutive set bits in w (highlighted by underline) is equal to $\texttt{cnt}(\texttt{map01}(w)) = 3$. Calling $\texttt{sel}$ on all set bits in $(\texttt{map01}(w)$ OR $\texttt{map10}(w) = \texttt{0010001010101001})$ yields the minimum range sequence of the column indices present in the bit vector; i.e. $[2, 5, 8, 9, 12, 14]$. Note that the upper bounds are substracted by one to represent closed intervals.

From a technical point of view, the following key design decisions are made to ensure space and time efficiency.

Non-blocking Parallel Access

All `scatter` operations for each pair of $[s, f]$ are computed in parallel across multiple threads. Concurrent write accesses to the bitvector can lead to race conditions depending on how computations are *partitioned* among threads. Different *partitioning schemes* might impose different requirements which will be explained in Section 4.3.2. If a race condition is likely in a particular partitioning, atomic operations are opted for all or partial parallel write accesses.

Similarly, the `gather` operations are done in parallel for each word. This requires some further considerations: for example, the starting index in the column indices array in which the minimum range sequence of the current word should be stored are not known until all previous words are processed. Instead of waiting for them to be processed, the starting index is re-calculated by each thread.

Apart from distributing `scatter` or `gather` operations among threads, BBB can benefit from another level of parallelism: vector parallelism, or single-instruction-multiple-data (SIMD), if supported by the underlying architecture. Vector parallelism allows increasing the effective word size by conducting `scatter` or `gather` operations simultaneously on multiple machine words. The length of SIMD instructions, i.e. the *vector length*, is architecture-dependent and usually matches the size of the cache line.

D.2 Index Calculation

For internal indexing, the bitvector is rearranged such that the first level $\mathcal{L}_0$ always comes first. Given b as the column index corresponding to the first bit in $\mathcal{L}_0$, the internal indexing is defined relative to b using modular arithmetic. To be specific, the *relative index* of column index j is defined as $r_j = (j - b) \bmod \mathcal{B}$; where $\mathcal{B}$ is the size of the bitvector which is the bandwidth. Consequently, the first relative indices—from 0 to $|\mathcal{L}_0|$—are assigned to $\mathcal{L}_0$, while the remaining indices are designated to $\mathcal{L}_1$. If the relative index is larger than $|\mathcal{L}_0|$, the corresponding bit is located in the second level with local index $r_i - |\mathcal{L}_0|$. Otherwise, it can be addressed by its relative index in $\mathcal{L}_0$. Figure 4b demonstrates the assignment of column indices in a row to each level (top), bitvector rearranged according to *relative indices* (middle), and the physical memory space corresponding to each level accessible with *local indices* (below).

Since modular arithmetic is expensive on GPUs, the relative index is calculated by $\mathcal{B} + j - b$ when $j < b$ and $j - b$ when $j >= b$. Although it imposes an additional conditional branch but it proved much more efficient in action. As stated before, the design is based on the fact that the probability of indices occurring in $\mathcal{L}_0$ is high. Given these circumstances, the conditional branches involved in calculating the local indices do not impede performance,

Algorithm 5 Bi-level Banded Bitvector `scatter` operation.

```
Require: Bi-level bitvector $\mathcal{B}$, start and finish column indices $s$ and $f$
1:  function SCATTER($\mathcal{B}$, $s$, $f$)
2:      $i \leftarrow \lfloor s/W \rfloor$                    ▷ Word index of the bit at $s$ in $\mathcal{B}$
3:      $j \leftarrow \lfloor f/W \rfloor$                    ▷ Word index of the bit at $f$ in $\mathcal{B}$
4:      $o \leftarrow s \bmod W$                              ▷ Offset of $s$ within word $i$
5:      $p \leftarrow f \bmod W$                              ▷ Offset of $f$ within word $j$
6:      $\mathrm{a} \leftarrow 2^w - 1$
7:      if $i = j$ then
8:          mask $\leftarrow$ SHIFTLEFT(SHIFTLEFT$(1, p - o + 1) - 1, o)$
9:          $\mathcal{B}$.XOR(mask, $i$)
10:     else
11:         mask $\leftarrow$ SHIFTLEFT(a, $o$)
12:         $\mathcal{B}$.XOR(mask, $i$)
13:         while $i < j$ do
14:             $i \leftarrow i + 1$
15:             $\mathcal{B}$.SETALLBITS($i$)
16:         mask $\leftarrow$ SHIFTRIGHT$(W - f - 1)$
17:         $\mathcal{B}$.XOR(mask, $i$)
```

Algorithm 6 Bi-level Banded Bitvector `gather` operation.

```
Require: Word $w$ and carried bit $c$
1:  function MAP10($w$, $c$)
2:      $x \leftarrow$ SHIFTLEFT$(w, 1)$ OR $c$               ▷ appending bit $c$ to $w$ and left-shift by 1
3:      report $x$ AND NOT$(w)$
4:  function MAP01($w$, $c$)
5:      $x \leftarrow$ SHIFTLEFT$(w, 1)$ OR $c$               ▷ appending bit $c$ to $w$ and left-shift by 1
6:      report $(w$ XOR $x)$ AND $w$

Require: Column indices subarray $C'_r$, bi-level bitvector $\mathcal{B}$, minimum and maximum column
         indices $j_{min}$ and $j_{max}$ in the row
7:  function GATHERSYMBOLIC($\mathcal{B}$, $j_{min}$, $j_{max}$)
8:      $b \leftarrow \lfloor j_{min}/W \rfloor$              ▷ Word index of the bit at $j_{min}$ in $\mathcal{B}$
9:      $e \leftarrow \lfloor j_{max}/W \rfloor$              ▷ Word index of the bit at $j_{max}$ in $\mathcal{B}$
10:     $z \leftarrow 0, \; c \leftarrow 0$
11:     for $i \in [b, e]$ do
12:         $z \leftarrow z + 2 * $ CNT(MAP01$(\mathcal{B}[i], c)$)
13:         $c \leftarrow$ RIGHTSHIFT$(\mathcal{B}[i], W - 1)$   ▷ $c$ is assigned to the most significant bit of $\mathcal{B}[i]$
14:     report $z$
15: function GATHERNUMERIC($C'_r$, $\mathcal{B}$, $j_{min}$, $j_{max}$)
16:     $b \leftarrow \lfloor j_{min}/W \rfloor$              ▷ Word index of the bit at $j_{min}$ in $\mathcal{B}$
17:     $e \leftarrow \lfloor j_{max}/W \rfloor$              ▷ Word index of the bit at $j_{max}$ in $\mathcal{B}$
18:     $k \leftarrow 0$
19:     for $i \in [b, e]$ do
20:         $w \leftarrow$ MAP01$(\mathcal{B}[i])$ OR MAP10$(\mathcal{B}[i])$
21:         for $j \in$ CNT$(w)$ do
22:             $C'_r[k] = (i \cdot W) +$ SEL$(w, j + 1)$
23:             $k \leftarrow k + 1$
```

as they follow an always-true pattern that is expected to be predicted correctly by the branch predictor.

E Partitioning Schemes

Despite the inherent differences in their design, computational hardware can be abstracted by a unified logical view. This abstraction allows us to effectively describe the partitioning schemes and the hierarchical parallelism inherent in multi-core and many-core architectures. Processing units typically comprise multiple or many *cores*, each of which is designed to execute multiple threads concurrently. In this unified computational model, a group of threads executing within a single core is termed a *team of threads* and the number of supported threads is called *team size*. Within a team, threads might share memory resources and be able to synchronize. Moreover, each thread might be capable of executing vector operations. Vector parallelism leverages the simultaneous processing of multiple data entries within a single instruction cycle (SIMD or vectorization on CPU and *warps* in GPU). The number of vector lanes that a thread can handle is defined as the *vector size*. We also define *block size* as the total parallel processing capability of a core; that is, *team size* × *vector size*.

Inspired by [13], we examined different strategies: *Thread-Sequential, Team-Sequential*, and *Thread-Parallel* partitioning schemes:

- **Thread-Sequential**: In this partitioning scheme, each team is responsible for computing a range of rows in **C**. These rows are distributed across threads in the team. To compute $C(i,:)$, a single thread *sequentially* iterates over non-zero ranges in $A(i,:)$. For each pair $[j,k]$ in $A(i,:)$, the thread accumulates all column indices corresponding to non-zero elements in $B(j,:)$ to $B(k,:)$. The accumulator exploits vector parallelism for storing each range in the accumulator. Since all threads work on different accumulators, there is no data race condition when accessing the accumulator. On the other hand, it requires more space as the number of active threads is high. This may be restrictive on GPUs for larger matrices as there are usually limited amount of global memory on devices.
- **Team-Sequential**: Despite Thread-Sequential partitioning, each team is assigned to a single row of **C** in this scheme. As suggested by the name, each team *sequentially* iterates over non-zero ranges in $A(i,:)$ as well as the corresponding rows in **B**. All threads in a team are assigned to different non-zero ranges within a single row of **B**. Similar to Thread-Sequential, `scatter` and `gather` operations on bitvector utilize vector parallelism. Since all team threads work on a row in **B**, there are fewer number of active rows compared to Thread-Sequential. Therefore, it has smaller memory footprint. However, when **B** is very sparse; i.e. there are few number of non-zero ranges in each row, this schemes may not fully utilize available computational resources.
  Moreover, as non-zero ranges in each row of B are disjoint, there is no race condition in row accumulation except for the first and the last words of each range. So, any bitwise operation on those words are atomic.
- **Thread-Parallel**: Similar to Team-Sequential, each team is assigned to compute a row of **C** in this scheme. However, each team sequentially traverses non-zero ranges in $A(i,:)$. For a pair $[j,k]$ in $A(i,:)$, all non-zero ranges from row $B(j,:)$ to $B(k,:)$ is distributed among threads. As a result, the chance of underutilization is less likely in this approach as long as the number of non-zero values (not ranges) is sufficiently large in **A**. As with previous approaches, threads use vector parallelism when computing each row of **B**.
  In terms of memory, this scheme is similar to Team-Sequential. However, since the accumulator is shared with multiple threads, all bitwise operations for row accumulation

Table 2 Chosen partitioning scheme and block sizes for different execution spaces.

Execution Space	Block size			Partitioning
	Team Size	Vector Size	Thread Work Size	
OpenMP (large graphs)	1	1	NA	`ThreadSequential`
OpenMP (small graphs)	1	1	NA	`ThreadParallel`
CUDA (large graphs)	32	32	$\omega^{1)}$	`ThreadSequential`
CUDA (small graphs)	8	8	8	`ThreadSequential`

1) $\omega = \frac{4n^2}{M}$; M = the size of global memory on GPU in bytes, n = size of the genome.

are atomic.

F Tuning Meta-parameters

We implemented the rSpGEMM algorithm with different partitioning schemes and evaluated the performance of each using various block sizes, as described in Section 4.3.2. In this work, we mainly report the performance of DiVerG with the best partitioning scheme and block size for each architecture. Table 2 summarizes the chosen partitioning and block sizes for each execution space and the size of input data. The implementation automatically decides these meta-parameters based on the underlying platform (CPU or GPU) and the input graph.

Given M is the size of global memory on GPU in bytes and $\mathcal{C}$ is the number of concurrent blocks that can be run on GPU, an input graph is considered *large* if its total sequence length is larger than $\frac{M}{4\mathcal{C}}$.

G Datasets Details

We performed our experiments using various pangenome graphs: mtDNA, BRCA1, LRC_KIR, MHC, B. *anthracis*, and the HPRC CHM-13 pangenome graph for regions chr1 and chr22. This section provides more details about the datasets. Table 3 presents some statistics of the sequence graphs used in our evaluation.

Table 3 Statistics of the sequence graphs used for performance evaluation.

Graphs	nodes[1)]	edges
mtDNA (GRCh37–1KGP)	21037	26842
BRCA1 (GRCh37–1KGP)	83267	85422
LRC_KIR (GRCh37–1KGP)	1108768	1154049
MHC-minigraph (GRCh38–alt)	10987753	11078552
B. *anthracis* (20 strains)	11237088	11253454
HPRC CHM13 chr22	63520037	63527923
HPRC CHM13 chr1	261344589	261360990

1) Note that all graphs are *character graphs*.

mtDNA graph

This graph is constructed using vg [20] and the mitochondrial DNA sequence in GRCh37 reference genome and small variants from the 1000 Genomes project (Phase 3) [1]:

```
$ vg construct \
      -r human_g1k_v37.fasta \
      -v ALL.chrMT.phase3_callmom-v0_4.20130502.genotypes.vcf.gz \
      -R MT > \
      ALL.chrMT.phase3_callmom-v0_4.20130502.genotypes.vg
```

BRCA1 gene graph

BRCA1 (BReast CAncer type 1) is a gene encoding breast cancer type 1 susceptibility protein. The human BRCA1 gene is located on the long (q) arm of chromosome 17 at region 2 band 1, from base pair 41 196 312 to base pair 41 277 500 (Build GRCh37/hg19). To ensure reproducibility, we re-used the BRCA1 gene graph that was previously published by PairG. It is a variation graph constructed using BRCA1 gene sequence from GRCh37 reference genome and the corresponding variants from 1000 Genomes Project:

```
$ vg construct \
      -r human_g1k_v37.fasta \
      -v ALL.chr17.phase3_shapeit2_v5b.20130502.genotypes.vcf.gz \
      -R 17:41196312-41277500 > \
      ALL.chr17-BRCA1.phase3_shapeit2_v5b.20130502.genotypes.vg
```

LRC_KIR graph

Leukocyte Receptor Complex (LRC) is a locus encoding a large number of immunoglobulin (Ig)-like receptors such as killer cell Ig-like receptors (KIR). In human genome, the LRC region is found at chromosomal region 19q13.4 and spans approximately 1Mbp. Similar to the mtDNA and BRCA1 graphs, this graph can also be constructed using the reference and variants in the 1000 Genomes Project:

```
$ vg construct \
      -r human_g1k_v37.fasta \
      -v ALL.chr19.phase3_shapeit2_v5b.20130502.genotypes.vcf.gz \
      -R 19:54528888-55595686 > \
      ALL.chr19-LRC_KIR.phase3_shapeit2_v5b.20130502.genotypes.vg
```

B. anthracis graph

For this dataset, a de Bruijn graph with a k-mer length of 25 is built using genomes of 20 different strains of B. *anthracis* and splitMEM [30]. The selected 20 strains are based on those reported by PairG and are listed in Table 4. The output of splitMEM is in DOT format and is converted to GFA with a simple Python script we implemented called `dot2gfa`, which is included with the DiVerG source code:

```
$ splitMEM -multiFa -file 20_strains.fna -mem 25
$ dot2gfa.py -k 25 -f 20_strains.fna --skip-loops cdg.dot
```

Table 4 List of 20 B. *anthracis* strains used to build the sequence graph.

Strain	Assembly id	Size (Mbp)
Ames	GCA_000007845.1	5.23
delta Sterne	GCA_000742695.1	5.23
Cvac02	GCA_000747335.1	5.23
Parent1	GCA_001683095.1	5.23
PR09-1	GCA_001683255.1	5.23
Sterne	GCA_000008165.1	5.23
CNEVA-9066	GCA_000167235.1	5.49
A1055	GCA_000167255.1	5.37
A0174	GCA_000182055.1	5.29
Sen2Col2	GCA_000359425.1	5.17
SVA11	GCA_000583105.1	5.49
95014	GCA_000585275.1	5.34
Smith 1013	GCA_000742315.1	5.29
2000031021	GCA_000742655.1	5.33
PAK-1	GCA_000832425.1	5.40
Pasteur	GCA_000832585.1	5.23
PR06	GCA_001683195.1	5.23
55-VNIIVViM	GCA_001835485.1	5.35
Sterne 34F2	GCA_002005265.1	5.39
UT308	GCA_003345105.1	5.37

MHC region graph

A graph for the major histocompatibility complex (MHC) region from reference genome and the corresponding alternative loci reported in GRCh38 [35]. Table 5 lists the sequenced used for construction of MHC graph. This graph, which is constructed based on pairwise alignments using minigraph [28] and seqwish [19], is served as a benchmark for comparing two methods as a mid-sized pengenome.

```
$ minimap2 -t 20 -cx asm20 *.fa | pigz > mhc-alts.pan.paf.gz
$ zcat mhc-alts.pan.paf.gz | fpa drop -l 10000 \
      | pigz > mhc-alts.pan.fpal10k.paf.gz
$ seqwish -s mhc-alts.pan.fa.gz -p mhc-alts.pan.paf.gz \
      -t 20 -b tmp/ -g mhc-alts.pan.fpal10k.gfa
```

HPRC CHM13 graph

To demonstrate the scalability and performance of the DiVerG in indexing large genome graphs, we employed the CHM13 reference graph released by the HPRC consortium from year 1 data [29]. The graph is built by minigraph [28] with CHM13+Y assembly as the reference [2].

[2] Accessible at: `https://github.com/human-pangenomics/hpp_pangenome_resources`

Table 5 The list of alternate loci used for construction of MHC graph.

NCBI Accession	GenBank Accession	Alternate Locus Group
NT_167244.2	GL000250.2	ALT_REF_LOCI_1
NT_113891.3	GL000251.2	ALT_REF_LOCI_2
NT_167245.2	GL000252.2	ALT_REF_LOCI_3
NT_167246.2	GL000253.2	ALT_REF_LOCI_4
NT_167247.2	GL000254.2	ALT_REF_LOCI_5
NT_167248.2	GL000255.2	ALT_REF_LOCI_6
NT_167249.2	GL000256.2	ALT_REF_LOCI_7
NT_187692.1	KI270758.1	ALT_REF_LOCI_8